Effect of Micro-patterned Mucin on Quinolone and Rhamnolipid Profiles of Mucoid *Pseudomonas aeruginosa* under Antibiotic Stress

Jin Jia[†⊥], *Dharmeshkumar Parmar*[‡⊥], *Joanna F. Ellis*[‡], *Tianyuan Cao*[†], *Allison R. Cutri*[†], *Joshua D. Shrout*[§&], *Jonathan V. Sweedler*[‡], *Paul W. Bohn*[*†£]

[†]Department of Chemistry and Biochemistry, University of Notre Dame, Notre Dame, Indiana 46556, United States

[£]Department of Chemical and Biomolecular Engineering, University of Notre Dame, Notre Dame, Indiana 46556, United States

[‡]Department of Chemistry and Beckman Institute for Advanced Science and Technology, University of Illinois at Urbana−Champaign, Urbana, Illinois 61801, United States

[§]Department of Civil and Environmental Engineering and Earth Sciences, University of Notre Dame, Notre Dame, Indiana 46556, United States

[&]Department of Biological Sciences, University of Notre Dame, Notre Dame, Indiana 46556, United States

[*]Author to whom correspondence should be addressed, *pbohn@nd.edu*.

ABSTRACT

Pseudomonas aeruginosa is commonly implicated in hospital acquired infections where its capacity to form biofilms on a variety of surfaces and the enhanced antibiotic resistance that results seriously limit treatment choices. Because surface attachment sensitizes *P. aeruginosa* to quorum sensing (QS) and induces virulence through both chemical and mechanical cues, we investigate the effect of surface properties through spatially-patterned mucin, combined with sub-inhibitory concentrations of tobramycin on QS and virulence factors in both mucoid and non-mucoid *P. aeruginosa* strains using multi-modal chemical imaging combining confocal Raman microscopy (CRM) and matrix-assisted laser desorption/ionization-mass spectrometry (MALDI-MS). Samples are comprised of surface-adherent static biofilms at a solid-water interface, supernatant liquid, and pellicle biofilms at an air-water interface at various time points. Although the presence of a sub-inhibitory concentration of tobramycin in the supernatant retards growth and development of static biofilms independent of strain and surface mucin patterning, we observe clear differences in the behavior of mucoid and non-mucoid strains. Quinolone signals in a non-mucoid strain are induced earlier and are influenced by mucin surface patterning to a degree not exhibited in the mucoid strain tested. Additionally, phenazine virulence factors, such as pyocyanin (PYO), are observed in the pellicle biofilms of both mucoid and non-mucoid strains, but are not detected in the static biofilms from either strain, highlighting the differences in stress response between pellicle and static biofilms. Differences between mucoid and nonmucoid strains are consistent with their strain-specific phenology, in which the mucoid strain develops highly protected biofilms.

KEYWORDS: biofilm, antibiotic resistance, *Pseudomonas aeruginosa*, mass spectrometry imaging, Raman imaging, rhamnolipids

The growing problem of antibiotic resistance has been linked to their extensive use, which enhances selection for multidrug resistant bacteria.[1] The tendency of bacteria to form biofilms, a dense assemblage of microbial cells in complex three-dimensional structures, greatly enhances their ability to resist antibiotics.[2] The extracellular polymetric substances (EPS) produced by biofilm-forming bacteria protect bacteria by acting as barrier for antibiotics, toxins, and host defense mechanisms. The complex structure of biofilms also provide an ideal microenvironment for microbial cells to exchange substances and acquire mutations that promote antibiotic resistance.[3-4] Biofilm formation is strongly linked with quorum sensing (QS), a mechanism by which bacteria regulate gene expression and which enables group behaviors in response to community-wide cellular density.[5-9] QS involves interconnected pathways that are sensitive to environmental cues and physicochemical properties of the host surface and these pathways are viewed as a potential drug target in addressing drug resistant bacteria.[10-13]

Pseudomonas aeruginosa, a Gram-negative opportunistic pathogen, is one of the most commonly found bacteria in hospital acquired infections, and it is capable of forming biofilms on a variety of surfaces.[14-15] *P. aeruginosa* possesses four interconnected QS systems: *las*, *rhl*, *pqs* and *iqs*, having characteristic signaling molecules associated with each.[16-17] The *pqs* system utilizes 2-alkyl-4-quinolones as QS mediators to control biofilm formation and some virulence genes, with over 50 quinolones having been detected in *P. aeruginosa*.[18-19] A hierarchical regulatory mechanism controls the four QS circuits in *P. aeruginosa*, with *las* inducing the expression of both the *rhl* and *pqs* systems and *pqs* positively regulating the *rhl* system.[17] On the other hand, *rhl* functions as a repressor of the *pqs* system and regulates the synthesis of rhamnolipids, which are amphipathic glycolipids with surfactant properties that can affect the structure of biofilms and eventually, their dispersal.[20-21] In addition, the regulation and actions of

QS can be altered by nutritional and environmental factors.[22-23] Further, the attachment surface and the spatial organization of bacterial cell clusters have also been found to impact biofilm development and function.[22, 24-26]

Different strains of *P. aeruginosa* produce one or more of three different polysaccharides named Pel, Psl, and alginate that comprise the substantive fraction of EPS in their biofilms. Alginate, specifically, is strongly linked to cystic fibrosis (CF) infection, as alginate overproduction is commonly observed in *P. aeruginosa* CF isolates, and these strains exhibit a mucoid phenotype caused by this alginate overproduction.[27] In this research, we have specifically studied two well-characterized *P. aeruginosa* strains. FRD1 is a CF lung isolate that was first identified because it displays a mucoid phenotype,[28] and numerous subsequent studies have highlighted different genetic and phenotypic aspects of alginate regulation and *P. aeruginosa* behavior for this strain.[29-33] PAO1C is wound isolate first described by Holloway [34-35] that has been used to detail many phenotypic behaviors; this strain does not exhibit a mucoid phenotype.[36-39]

Also of particular relevance to cystic fibrosis, *P. aeruginosa* biofilm development is known to be influenced by mucin, a lung glycoprotein that is a key component of airway fluid. Numerous studies have identified that *P. aeruginosa* shows a mucin-specific adhesion mechanism that greatly enhances biofilm development and resistance to antibiotics.[22, 24, 26, 40] More specifically, previous work from the authors' laboratories demonstrated that well-defined spatial patterning of biopolymers affects the production of signaling molecules and biofilm growth in both mucoid and non-mucoid strains of *P. aeruginosa*.[24]

Exposure to the antibiotic tobramycin, even at subinhibitory concentrations, has been shown to impair *P. aeruginosa* biofilm formation and increase susceptibility to other antibiotics.

[41] However, the spatial growth and molecular profile of *P. aeruginosa* under the influence of antibiotics is poorly characterized, so here we explore the effect of surface mucin patterning on the ability of *P. aeruginosa* to resist antibiotics exposure at sub-inhibitory concentration. We evaluate *P. aeruginosa* biofilm formation on unpatterned and patterned mucin surfaces in the presence of tobramycin at sub-inhibitory concentrations to understand how the combination of the presence and presentation of surface mucin and drug exposure influence biofilm formation, maturation, and dispersal by monitoring key signaling molecules and virulence factors secreted by *P. aeruginosa*, along with its cell density in supernatant medium over time. We combine confocal Raman microscopy (CRM) and matrix-assisted laser desorption/ionization-mass spectrometry (MALDI-MS) to capture the spatial distribution of secreted *pqs* signaling molecules and rhamnolipids from static biofilms at three distinct locations – (1) at the solid-liquid interface, (2) in the supernatant above the biofilm, and (3) in pellicle biofilms which are formed at the liquid-air interface - to investigate the interaction between *rhl* and *pqs* QS circuits in *P. aeruginosa* under antibiotic stress. The abundances of C_7 (2-heptyl-3-hydroxy-4(1*H*)-quinolone) and C_9 (2-nonyl-3-hydroxy-4(1*H*)-quinolone) alkyl quinolones (AQs), along with their respective structural isomers 2-heptyl-4-hydroxyquinolone *N*-oxide (HQNO) and its C_9 side chain variant 2-nonyl-4-hydroxyquinolone *N*-oxide (NQNO), are characterized as a function of mucin surface patterning and tobramycin exposure for various biofilm samples. Additionally, four congener classes of rhamnolipids (di-rhamno-di-lipid, di-rhamno-mono-lipid, mono-rhamno-di-lipid, mono-rhamno-mono-lipid) are profiled by MALDI-MS and the overall composition and relative rhamnolipid profiles are compared as a function of biofilm conditions, highlighting the most relevant rhamnolipids. The impact of mucin patterning on quinolone and

rhamnolipid profiles for *P. aeruginosa* strains under antibiotic stress reveals profound differences between strains exhibiting mucoid and non-mucoid phenotypes.

RESULTS AND DISCUSSION

Detection of Biomolecules by CRM and MALDI FT-ICR MS. Responses of several biofilm phenotypes were examined as a function of time to sub-lethal exposure to the antibiotic tobramycin. After 1 h incubation in minimal-glucose medium without tobramycin, static bacterial biofilms from both FRD1 and PAO1C strains and in the presence of patterned and unpatterned mucin were transferred into minimal-glucose medium in the presence of 5 μg mL^{-1} tobramycin and incubated for 48, 72, and 96 h, as shown in **Figure S1**. In order to assess the ability of both cells and soluble factors to move from the immersed biofilm samples to the

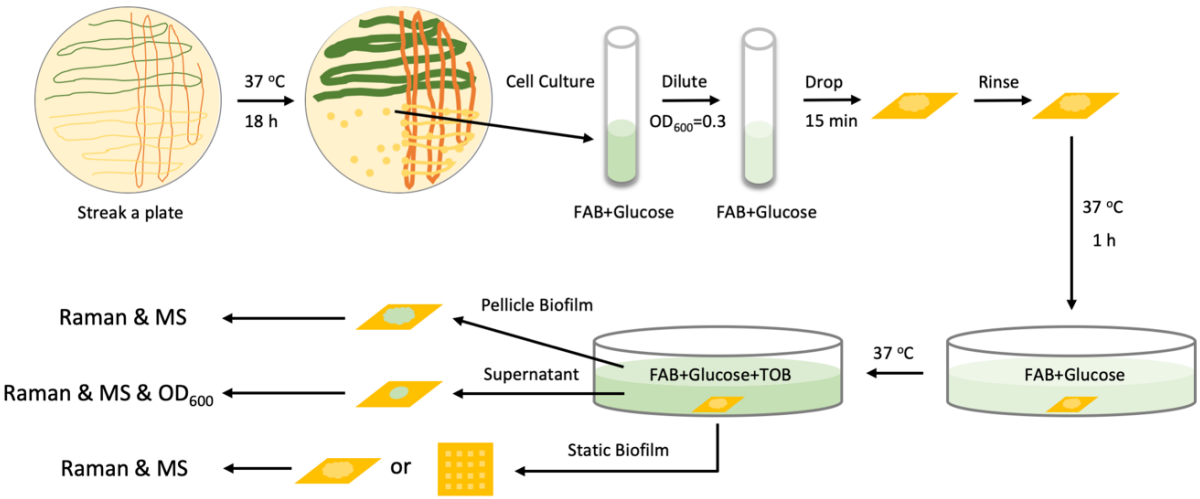

Figure 1. Schematic diagram illustrating sample preparation for analytical characterization and chemical imaging of biofilm samples. Static biofilm samples were acquired from the solid-liquid interface, and pellicle biofilm samples from the air-water interface. Static biofilms were grown in the presence of both patterned and unpatterned mucin on gold-coated Si.

supernatant and pellicle biofilms, samples for analysis were collected from the pellicle biofilms,

bacteria-free supernatant and static biofilms at the air-liquid interface, supernatant liquid, and solid-liquid interface, respectively, as shown schematically in **Figure 1**. Samples acquired from the time points mentioned above (48, 72, 96 h) were subjected to multi-modal imaging analysis. The OD_{600} values of bacterial cultures were monitored during the bacterial incubation, as shown in **Figure S2**. Representative CRM Raman images and principal component analysis (PCA) data from the three types of *P. aeruginosa* samples are shown in **Figure S3**. By comparing features in the PCA loading plots in **Figure S3** from the bacterial samples with the Raman features from chemical standards in **Table S1**, four classes of biomolecules widely reported in *P. aeruginosa* are identified, namely, 2-nonyl/heptyl-4-hydroxyquinoline N-oxide (N/HQNO), 2-heptyl/nonyl-3-hydroxy-4-quinolone (C_7/C_9-PQS), phenazine-1-carboxylic acid (PZCA) and pyocyanin (PYO). Visual inspection of the PCA loading plots from bacterial samples and Raman features from chemical standards shows distinct patterns for each class of biomolecules that were used to elucidate *P. aeruginosa* QS behaviors.

Alkyl quinolones produced by two phenotypically distinct strains of *P. aeruginosa* were also probed using MALDI FT-ICR MS in targeted MS/MS imaging mode. 2-heptyl-3-hydroxy-4-quinolone known as pseudomonas quorum sensing molecule (C_7-PQS) associated with group behavior and biofilm formation in *P. aeruginosa* and its homologue, C_9-PQS, were differentiated from their respective structural isomers HQNO and NQNO using unique product ions at *m/z* 159.067 and *m/z* 175.062.[42-43] Extracted ion profiles generated using ±5 ppm window around these *m/z* were used to create the spatial distribution profile of these molecules on the sample surface. HQNO and NQNO are two of the many 2-alkyl-4-quinolone N-oxides (AQNOs) classes of molecules that are most abundant and have been reported to exert antibiotic effects through cytochrome inhibition, and are relevant in bacterial interactions with other species.[44]

As shown in **Figure 1**, patterned/unpatterned bacterial biofilms were transferred and immersed in minimal-glucose medium containing tobramycin (5 μg/mL) and incubated at 37 ºC for various periods of time. Compared to the biofilms grown without tobramycin, the growth of both strains on patterned/unpatterned mucin surfaces is greatly reduced under tobramycin treatment.[24] Also, the measured OD_{600} values in **Figure S2** stayed close to zero at $t \leq 24$ h incubation time for all four conditions, indicating a negligible number of detached bacterial cells in the medium. Starting at 48 – 72 h incubation time, the OD_{600} values for all four media begin to deviate from zero, and at 72 h increased optical density was measured under all four experimental conditions. Independent of mucin patterning, the FRD1 samples showed very similar OD_{600} values as a function of incubation time, indicating that growth and detachment of planktonic cells was largely unaffected by the spatial patterning of the mucin surfaces. In contrast, the non-mucoid PAO1C strain exhibited markedly different behavior, with the OD_{600} values on patterned mucin indicating faster accumulation of planktonic cells (by a combination of growth-and detachment) and pigment secretion in comparison to the FRD1 strain. The PAO1C strain exhibited much slower growth on the unpatterned mucin surface up to 84 h, before eventually reaching the same optical density as that on patterned mucin at 96 h. Clearly, these two strains exhibit marked differences in response to spatial patterning.

To better understand *P. aeruginosa* biofilm growth on patterned/unpatterned mucin surfaces in the presence of the antibiotic tobramycin, secreted molecular factors obtained from static biofilms, the bacteria-free supernatant, and pellicle biofilms were compared using CRM, as shown in **Figure S3**. A typical progression during *P. aeruginosa* community development in static biofilms proceeds by initial appearance of N/HQNO and then PQS. In our previous work, mucoid FRD1 static biofilm samples exhibited N/HQNO at 24 h and both N/HQNO and PQS at

48 h on both patterned/unpatterned mucin surfaces in the absence of tobramycin treatment.[24] However, in the presence of tobramycin, AQ metabolites were not detected from PAO1C

Table 1. Biomolecules detected from mucoid FRD1 samples by CRM[a]

	Mucin			P-Mucin		
Time	Pellicle	Supernatant	Static	Pellicle	Supernatant	Static
48 h	-	Salt	Salt	-	Salt	Salt
72 h	-	Salt	Salt	-	Salt	Salt
96 h	PYO, PQS	PYO	PQS	PYO, PQS	Salt	HQNO, PQS

[a] Entries for an AQ or phenazine indicates that PCA gave a Z-score plot matching the Raman spectrum of that component's standard. C_7- and C_9-congeners are indistinguishable by CRM, so entries do not distinguish between HQNO/NQNO and C_7/C_9-PQS.

Table 2. Biomolecules detected from non-mucoid PAO1C samples by CRM

	Mucin			P-Mucin		
Time	Pellicle	Supernatant	Static	Pellicle	Supernatant	Static
48 h	-	Salt	Salt	-	Salt	HQNO
72 h	-	Salt	Salt	-	Salt	HQNO, PQS
96 h	PYO	PZCA	PQS	PYO	PYO	PQS

samples until 72 h (on patterned surfaces) and until 96 h for FRD1 samples on either patterned or unpatterned mucin surfaces, as shown in **Table 1**. This observation is consistent with the OD_{600} measurements indicating that tobramycin substantially slows the growth of static biofilms that exhibit a mucoid phenotype. At 96 h (**Table 1**), static biofilms of the FRD1 samples show only PQS on unpatterned mucin, while N/HQNO and PQS are both detected on patterned mucin, suggesting that discrete patterning of mucin slows the transition of static biofilms formed by the

mucoid strain to a mature state, relative to the biofilms of the same strain on unpatterned mucin. In contrast, static biofilms formed by the non-mucoid strain PAO1C exhibit N/HQNO at 48 h and N/HQNO with PQS at 72 h, while maturing to a chemical state exhibiting predominantly PQS at 96 h on patterned mucin surfaces in the presence of tobramycin. However, PQS was not detected until 96 h on unpatterned mucin, consistent with the slower rise of the OD_{600} values of the supernatant medium in contact with the non-mucoid PAO1C strain on unpatterned mucin.

Distinctive quinolones profiles detected in the static biofilms formed by mucoid vs. non-mucoid P. aeruginosa strains. MSI revealed different heterogenous spatial distribution patterns for AQ and AQNO molecules in static biofilms produced by these two strains. Changing distribution patterns over 48, 72, and 96 h indicated dynamic abundance of all four molecules in static biofilm samples (**Figure S4**). As shown in **Figure 2**, both alky quinolones and alkyl quinolone *N*-oxides are present in higher
abundance in PAO1C in comparison to FRD1 samples at 48 h, signifying early induction of alkyl quinolone production (and likely PQS quorum sensing) on both unpatterned and patterned surfaces, consistent with the CRM results summarized in **Tables 1** and **2**. However, at 72 and 96 h, in agreement with the OD_{600} behavior shown in **Figure S2**, FRD1 samples show an increasing abundance of quinolones, indicating activation of biosynthetic pathways for quinolone synthesis after an initial delay.

Figures 2(A) and **2(B)** show relative signal abundance of PQS and C_9-PQS, respectively. Interestingly, the FRD1 samples show increasing signal abundance of AQs over time, independent of the mucin surface, in comparison to the PAO1C strain, where profiles of both AQs are influenced by the type of mucin surface, with the patterned surfaces exhibiting an intensity maximum at 72 h. PQS abundance is also highest in 96 h FRD1 biofilms in comparison

to other static biofilms, whether from mucoid or non-mucoid strains. In contrast, PQS abundance in PAO1C biofilms, which increases marginally over time on unpatterned mucin, is elevated on the patterned mucin surface. Unpatterned mucin leads to relatively stable C_9-PQS spatial abundance in non-mucoid PAO1C samples at all time points, **Figure 2(B)**, whereas, patterned mucin resulted in the highest signal intensity of C_9-PQS at 72 h across all static biofilm samples.

Relative signal abundances of *N*-oxides, HQNO (*m/z* 260→159) and NQNO (*m/z* 288→159) in static biofilm samples are depicted in **Figures 2(C)** and **2(D)**, respectively. Both molecules show similar trends within each sample category, suggesting that the biosynthesis of

(A)

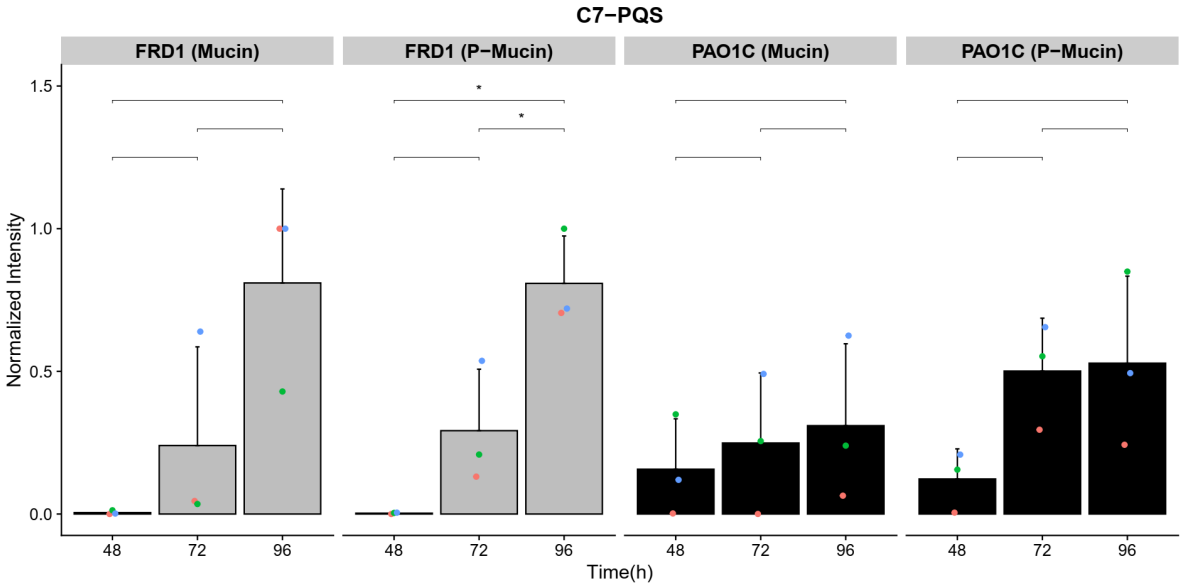

(B)

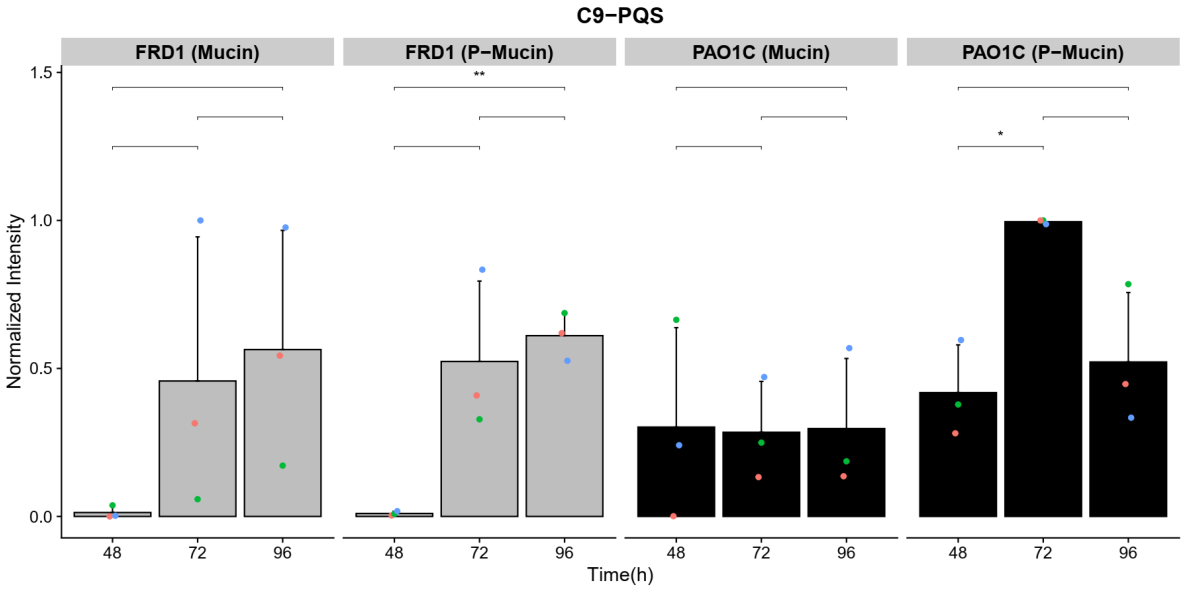

(C)

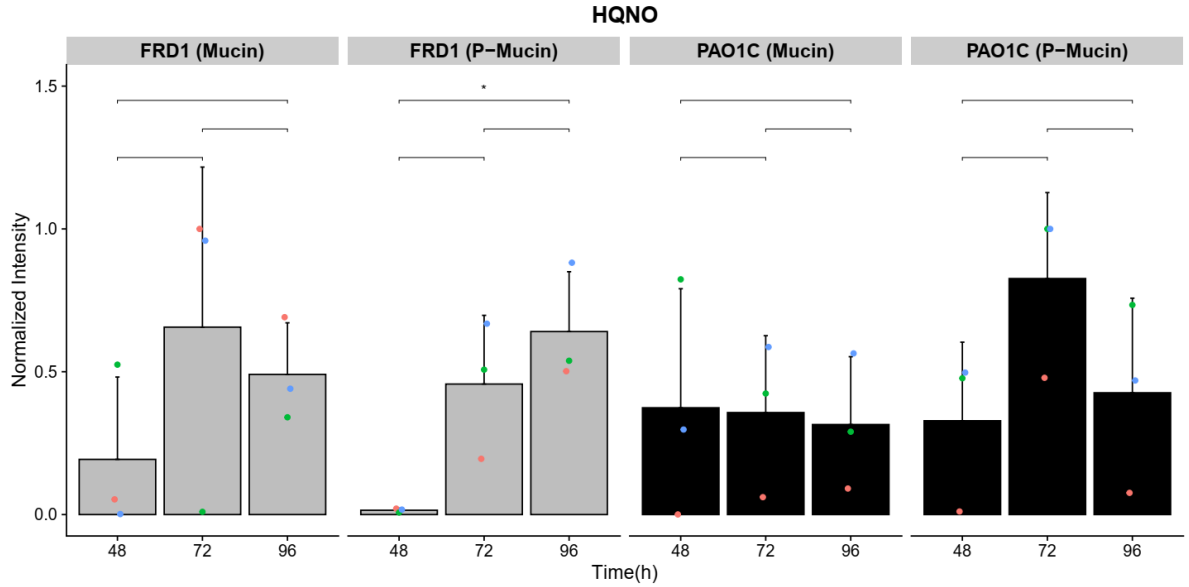

(D)

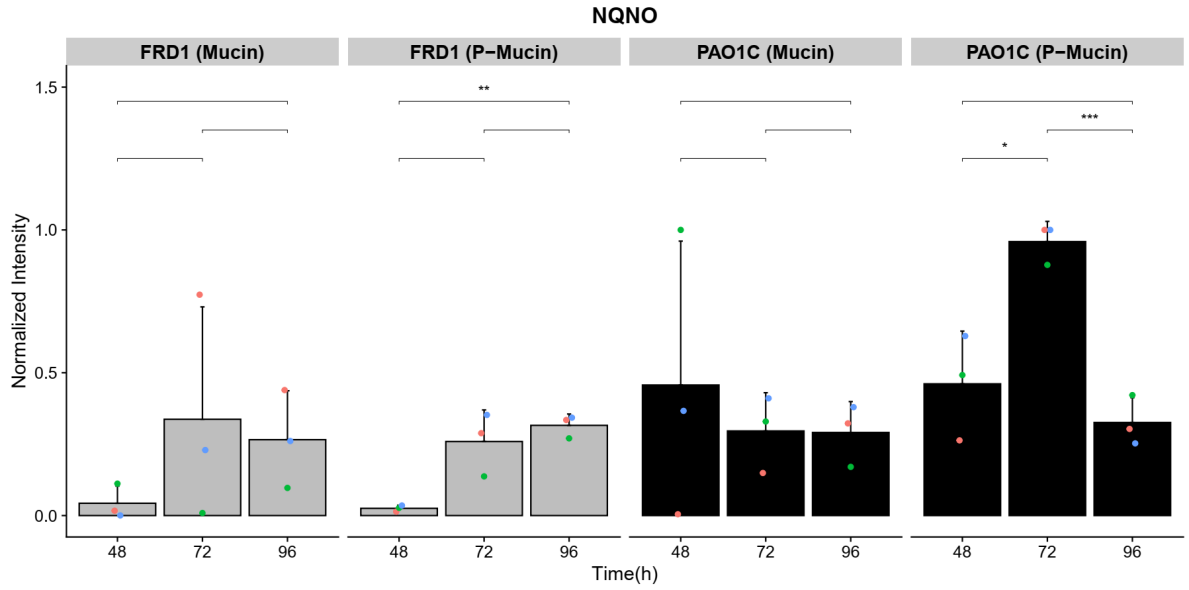

Figure 2. Relative abundance of AQ and AQ N-oxide molecules in static biofilms of mucoid (FRD1) and non-mucoid (PAO1C) *P. aeruginosa* strains grown on unpatterned mucin (Mucin) and patterned mucin (P-Mucin) surfaces. Relative ion abundances for (a) C_7-PQS (*m/z* 260 → 175), (b) C_9-PQS (*m/z* 288 → 175), (c) HQNO (*m/z* 260 → 159) and (d) NQNO (*m/z* 288 → 159) at 48, 72, and 96 h measured from static biofilm samples using MALD-MS imaging.

Average intensity values are normalized to the maximum value for each molecule across all samples within a biological replicate. The error bars represent standard deviation of three biological replicates. Colored dots represent individual biological replicates. Horizontal bars indicate time-point samples tested for statistical significance using Student's t-test (n = 3, unpaired, two tailed). P-values derived from these comparisons are highlighted with asterisk (* = $p < 0.05$, ** = $p < 0.01$, *** = $p < 0.001$, No label = $p > 0.05$).

HQNO and NQNO is correlated and relatively independent of mucin patterning. FRD1 biofilms grown on unpatterned mucin show higher levels of both molecules with maximum expression at 72 h, whereas biofilms grown on patterned mucin show increased abundance of both N-oxide congeners through 96 h, consistent with the interpretation above that patterning retards development of the mature phase characterized by high PQS abundance. Expression of AQNOs in biofilms of the non-mucoid PAO1C strain formed on mucin surfaces are comparable across all three time points in each mucin category.

The two most important findings of these MSI experiments are: (1) the diminished signals from FRD1 biofilms, and (2) the transient rise of the N-oxides at intermediate times in the non-mucoid PAO1C strain. Both observations are in agreement with the CRM imaging results reported in static biofilm column of **Tables 1** and **2**. Furthermore, and again consistent with CRM results, patterned mucin surfaces accentuate the transient rise of N-oxides. This also agrees with previous observations from our laboratories regarding the temporal evolution of non-mucoid *P. aeruginosa* biofilms in the absence of mucin or surface patterning.[45]

Quinolone profiles in pellicle biofilms and supernatant. In physical configurations such as the one used in this experiment, the static biofilm and pellicle biofilm can communicate chemically through the supernatant liquid medium. However, the pellicle biofilms behave in a way that is

distinctly different from the static biofilms. At 96 h, PYO is detected under a range of conditions, both in the supernatant and in pellicle biofilms. PYO is identified in the presence of (*a*) both patterned and unpatterned mucin static biofilm surfaces, and (*b*) for both mucoid FRD1 and non-mucoid PAO1C strains, as shown in **Tables 1** and **2**. In addition, while, PYO is observed in the supernatant and in pellicle biofilms, it is never observed in the static biofilms. In addition, the supernatant in contact with PAO1C samples, shows the presence of virulence factors PZCA (unpatterned) or PYO (patterned), suggesting that these factors are secreted and subsequently transported in the supernatant. There are two putative origins for the phenazine virulence factors, either the static or pellicle biofilm. However, PYO is observed in the pellicle biofilms of both FRD1 and PAO1C strains, and remains undetected in the static biofilms from both strains. This strongly suggests that the pellicle biofilm is the origin of the phenazines, which are then transported into the contacting supernatant. These observations highlight the clear differences in QS response exhibited by pellicle and static biofilms. Furthermore, they are consistent with previous observations from our laboratories that PQS is upregulated in the presence of environmental stressors.[38]

MS imaging also shows the presence of AQs and AQNOs in both pellicle biofilms and supernatant samples collected at 96 h from FRD1 and PAO1C biofilm cultures, highlighted by the presence of PQS, C_9-PQS, HQNO, and NQNO in **Figure 3**. Pellicle biofilms exhibit more abundant AQs and AQNOs in comparison to the supernatant under all four experimental conditions, which is understandable given the large difference in volumes of the two environments. Maximum signal intensities for AQs were observed in pellicle samples collected from PAO1C samples grown on patterned mucin, followed by that from uniform mucin, see **Figures 3** and **S4**. Pellicle biofilms also show different PQS profiles than static biofilms where FRD1 samples exhibit

higher PQS signals than PAO1C samples. However, similar to the behavior in static biofilms, the AQ profile in FRD1 is relatively insensitive to mucin surface characteristics, while patterned mucin increases AQ production in PAO1C samples.

It is also apparent that the AQ signal intensities in supernatant samples are greatly diminished relative to pellicle biofilms as evident from the *y*-axis scales for the supernatant samples in **Figures 3(A)** and **3(B)**. This likely reflects a combination of limited secretion of these

(A)

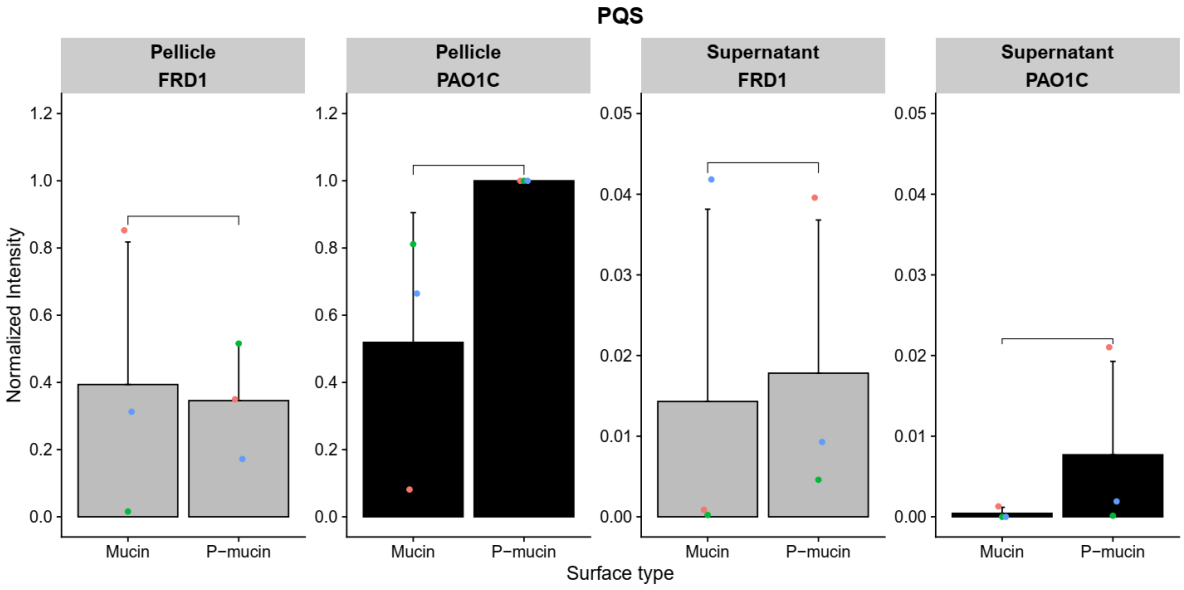

(B)

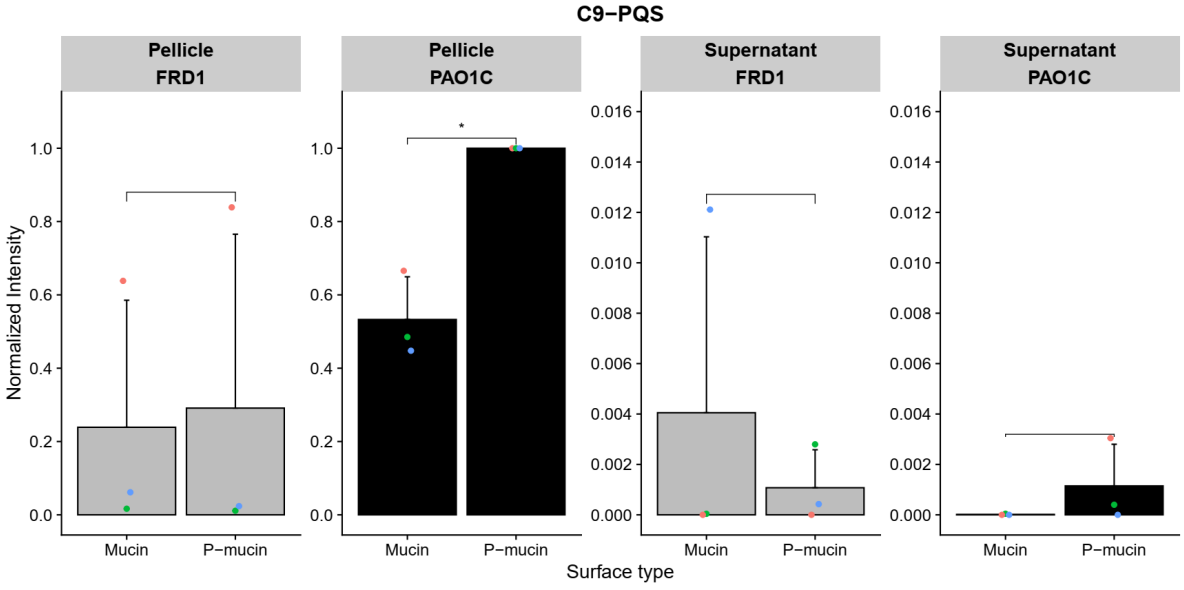

(C)

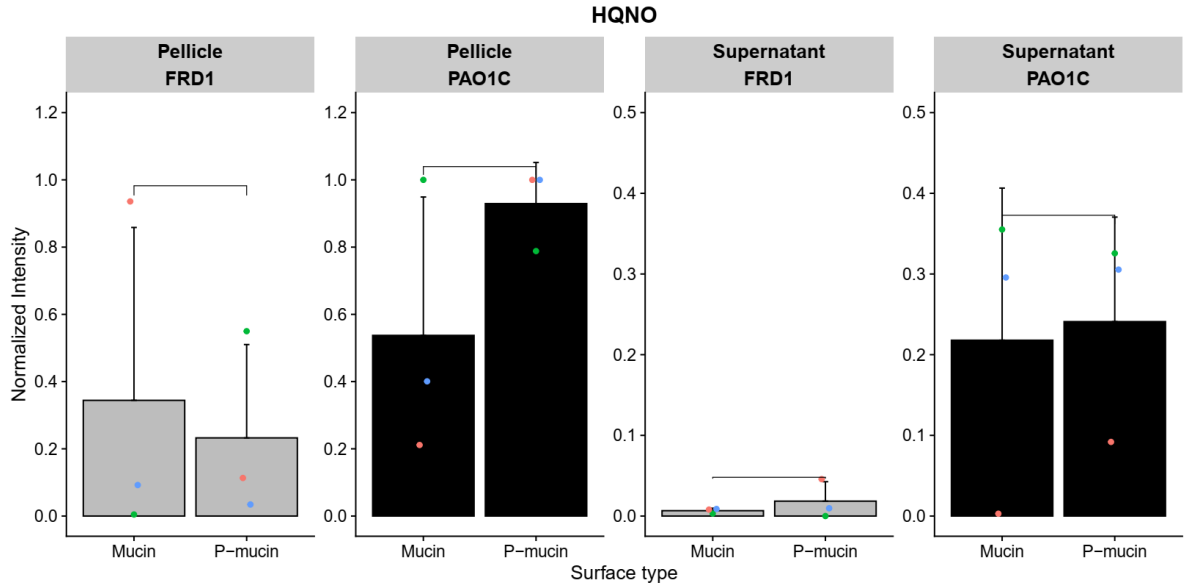

(D)

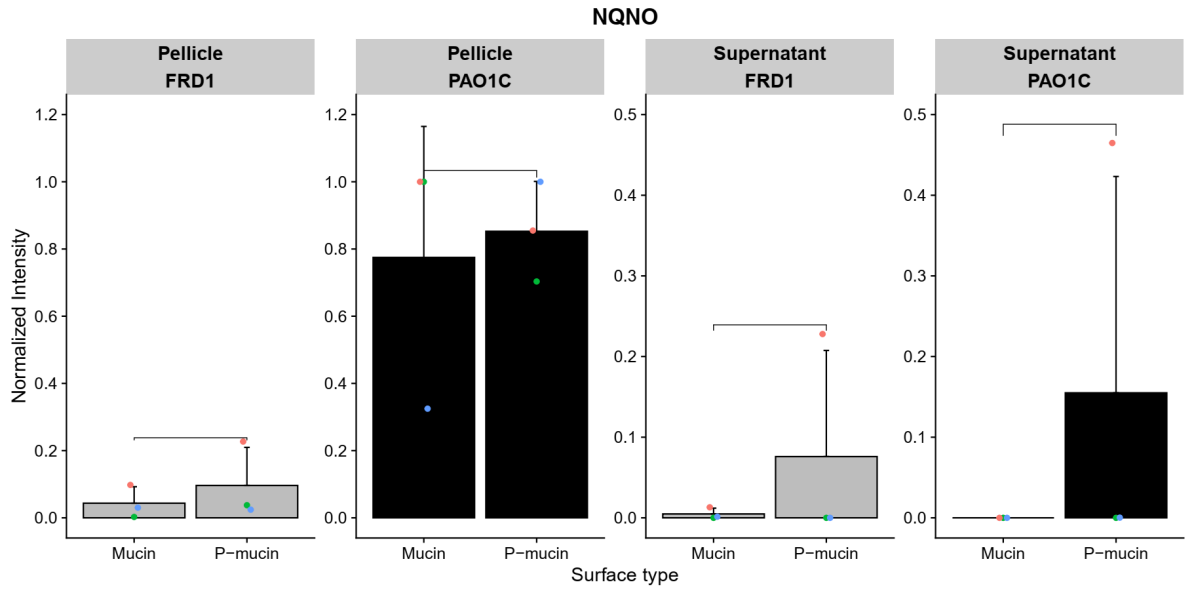

Figure 3. Relative ion abundances of AQs and AQNOs in pellicle biofilms and supernatant samples collected at 96 h from mucoid (FRD1) and non-mucoid (PAO1C) *P. aeruginosa* strains grown on unpatterned (Mucin) and patterned (P-Mucin) mucin surfaces. Relative ion abundances of (a) PQS (*m/z* 260 → 175), (b) C_9-PQS (*m/z* 288 → 175), (c) HQNO (*m/z* 260 → 159) and (d) NQNO (*m/z* 288 → 159) estimated using MALDI-MS imaging. Average intensity

values are normalized to the maximum value for each molecule across all samples within a biological replicate. The error bars represent standard deviation of three biological replicates. Colored dots represent individual biological replicates. Supernatant data are magnified to facilitate visual comparison. Horizontal bars indicate group tested for statistical significance using Student's t-test (n = 3, unpaired, two tailed). P-values derived from these comparisons are highlighted with asterisk (* = $p < 0.05$, No label = $p > 0.05$).

molecules into the supernatant and the dilution effect caused by the larger volume of the supernatant. However, the source of the AQ signal is difficult to ascertain, as it could be derived from planktonic cells or from the pellicle or static biofilms, individually or collectively. The AQNOs, however, tell a different story. HQNO and NQNO MALDI-MS signals are uniformly higher in both supernatant and pellicle biofilms from the PAO1C strain, consistent with its transient increase at intermediate times (**Figure 2**) and the CRM data in **Table 2**.

Rhamnolipid expression. Separately, high resolution MS imaging data acquired in the *m/z* 100-1100 window reveal the presence of various rhamnolipid congeners in these static biofilms. From a targeted screening list containing 174 adducts ($[M+H]^+$, $[M+Na]^+$, $[M+K]^+$) of 58 different mono- and di-rhamnolipid congeners, 38 adducts (**Table S2**) are detected within ±5 ppm mass accuracy for PAO1C. The percentage of rhamnolipids adducts observed as $[M+H]^+$, $[M+Na]^+$, $[M+K]^+$ is 15.8, 47.4 and 36.8, respectively.[46] PCA of static biofilm samples (all time points, 3 biological replicates) reveals the *m/z* values that contribute most towards principal component 1 (PC1) and principal component 2 (PC2). **Figure 4** shows a plot of PC1 *vs.* PC2 for 72 h and 96 h static biofilm samples for the most intense 23 *m/z* values. PC1 and PC2 capture 81.5 and 11.5% variation from the rhamnolipid data, respectively and account for 93% of the variance in

combination. As expected, static biofilms are most differentiated by PC1. Samples are distinctly grouped by strain type and time point in **Figure 4**.

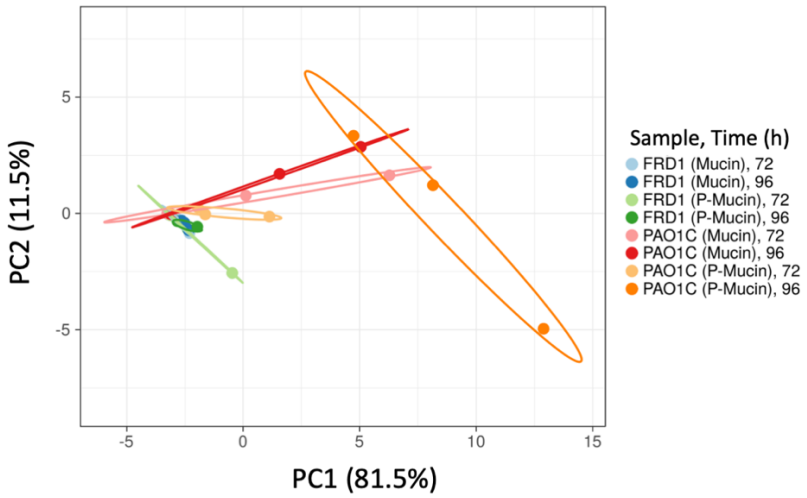

Figure 4. Principal component analysis (PCA) of 23 rhamnolipid adduct *m/z* values as exemplified the two largest principal components, PC1 and PC2, in 72 h and 96 h time points from static biofilms. The wider distribution of non-mucoid (PAO1C) samples (red, orange) indicates higher rhamnolipid production in comparison with the mucoid (FRD1) strain (blue, green). The 96 h non-mucoid biofilm grown on P-mucin surface showed the highest relative abundance of rhamnolipid.

PAO1C biofilms are markedly grouped from FRD1 samples. Interestingly, PAO1C biofilms show the highly differentiated profiles of rhamnolipids, and show that rhamnolipid expression is altered by the type of mucin surface. Specifically, the 96 h non-mucoid biofilm grown on patterned mucin exhibits consistently high rhamnolipid signals. FRD1 samples, on the other hand, show rhamnolipid signal behavior that varies little with mucin surface patterning or time, reflecting the relatively low level of rhamnolipid synthesis in this strain. Rhamnolipids were further analyzed by deconvoluting the observed adducts into individual rhamnolipid congeners followed by estimation of their cumulative abundance in each category.

Figure 5 illustrates the combined profile of rhamnolipids in four congener categories: **(A)** mono-rhamno-mono-lipid **(B)** mono-rhamno-di-lipid **(C)** di-rhamno-mono-lipid **(D)** di-rhamno-di-lipid. Rhamnolipid signals are strongly elevated in the non-mucoid strain, with highest signal

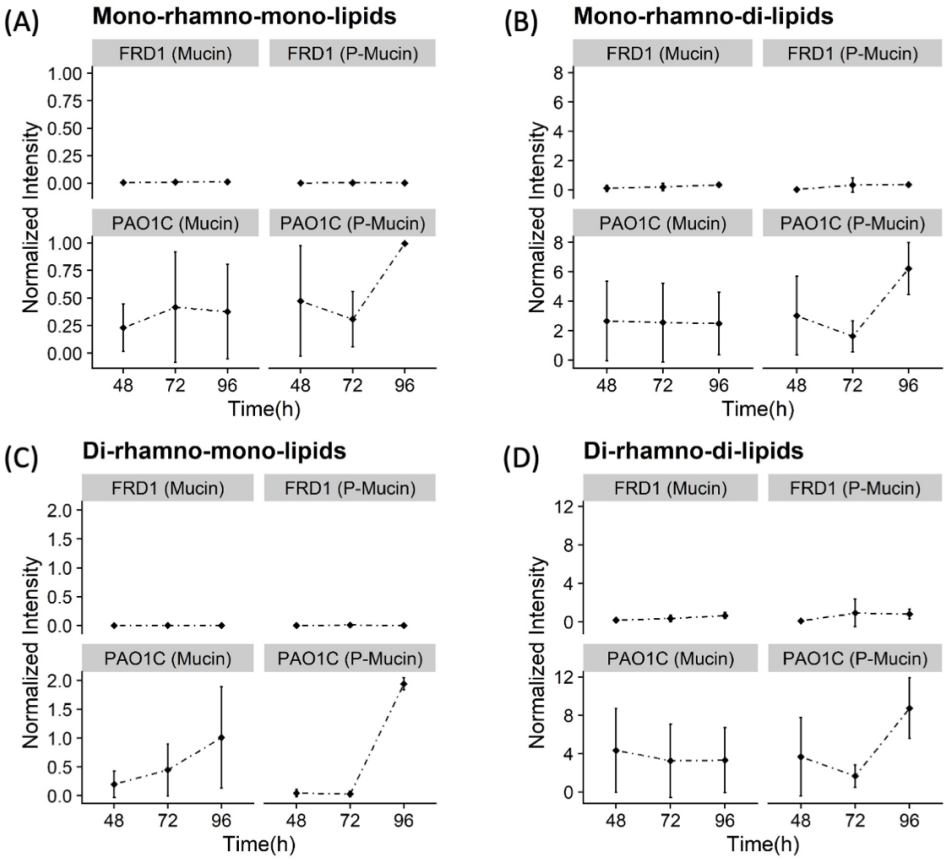

Figure 5. Relative abundances of rhamnolipid classes in static biofilm samples. Rhamnolipid data is grouped into four congener classes: (A) mono-rhamno-mono-lipid (B) mono-rhamno-di-lipid (C) di-rhamno-mono-lipid (D) di-rhamno-di-lipid. Top panel: mucoid strain (FRD1), bottom panel: non-mucoid strain (PAO1C).

abundance in 96 h biofilms grown on patterned mucin in each congener category. Rhamnolipid profiles from pellicle biofilms and supernatant samples at 96 h are consistent with the rhamnolipid profiles in static biofilm samples. **Figure 6** shows normalized signal intensities of the highly differentiated rhamnolipid adducts from static biofilms by congener category,

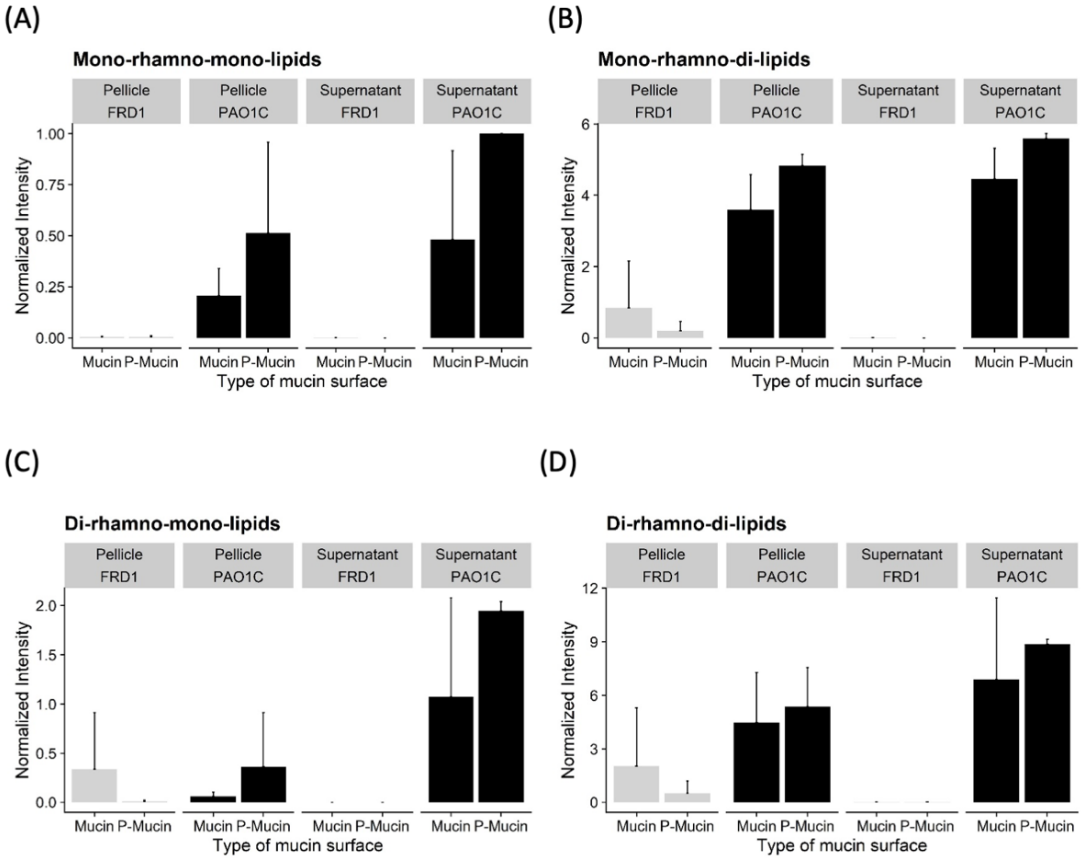

Figure 6. Comparison of rhamnolipid profiles of the highly differentiated rhamnolipid adducts in pellicle biofilm and supernatant samples collected at 96 h. Average intensities from three biological replicates are compared. Error bar represents standard deviation of average intensities. Grey and black bars represent pellicle biofilm and supernatant from mucoid (FRD1) and non-mucoid (PAO1C) strains, respectively.

when these are measured in pellicle biofilms and supernatant samples. Rhamnolipid expression is again consistently higher in PAO1C biofilms and supernatants than the corresponding FRD1 biofilm samples. Interestingly for the PAO1C, higher amounts of rhamnolipids are observed in the supernatant as compared to the pellicle biofilms and these levels are further elevated by patterned mucin surfaces. In contrast, higher signal intensities of rhamnolipids were observed in mucoid pellicle biofilms from the FRD1 strain in comparison to its supernatant samples.

Implications for P. aeruginosa collective behavior. A number of studies suggest that biofilms augment bacterial resilience against antimicrobials and host immune system in comparison to the planktonic state.[47-49] Understanding the impact of currently used antimicrobials on quorum sensing signaling molecules and other bacterial products of quinolone and rhamnolipid class serves the broad goal of understanding clinically relevant biofilms.[50-51] Bacteria deploy various classes of molecules to ensure growth and survival in the presence of host tissue. Quorum sensing is one of key contributor in this process that enables formation of biofilms upon sensing a requisite level of signaling molecules.[9, 12, 18] Because prior studies of biofilms have highlighted the combined impact of drug exposure and the physical structure of the local environment on secretion of molecular factors in *P. aeruginosa*,[11, 52] we initiated the current study to characterize the secretion of quinolones, phenazines, and rhamnolipids in two strains known to exhibit mucoid and non-mucoid phenotypes under controlled exposure to an antibiotic and with surface patterning of mucin.

Unique distribution patterns indicate differences in onset, localization, and dynamic spatial abundance of quinolones over the 48 – 96 h post-deposition period. The results clearly indicate that quinolone signals in PAO1C samples are induced earlier and are influenced by mucin surface patterning to a degree not exhibited in the FRD1 strain. Additionally, pellicle biofilms derived from PAO1C samples in the presence of patterned mucin show the highest level of quinolone signals. FRD1 biofilms, on other hand, are relatively uninfluenced by mucin surface patterning. Quinolone signals observed in the supernatant are a fraction of that in pellicle biofilm. This suggests that the quinolone signal localization is largely controlled by cellular secretion in the immediate microenvironments. We also observe a correlation between rhamnolipid content and OD_{600} reading of supernatant samples suggesting that rhamnolipids are important for biofilm dispersal.[53-54] Rhamnolipids have been associated with open channel formation as well as bacterial

cell attachment with the biofilm architecture, thereby influencing cell-to-cell interactions.[55] Open channels could allow better nutrient exchange and support bacterial growth. Furthermore, dissociation of adherent cells into the planktonic state may increase bacterial cell migration leading to higher cell densities in culture medium. Both phenomena are consistent with their strain-specific phenology, in which the mucoid strain develops highly protected biofilms.

CONCLUSIONS

The present study highlights how quinolones and rhamnolipid profiles vary among three different sectors – static biofilm at the solid-liquid interface, supernatant liquid, and pellicle biofilm at the air-water interface, in a complex three-dimensional environment. Multi-modal chemical imaging reveals variations in the spatial distribution and relative abundance of secreted AQ and AQNO molecules on biofilm surfaces in two phenotypically distinct, *i.e.*, mucoid and non-mucoid, *P. aeruginosa* strains developed on unpatterned mucin and patterned mucin surfaces while being exposed to tobramycin at sub-inhibitory concentration. The present study reveals four key aspects of *P. aeruginosa* behavior under these conditions. First, the presence of a sub-inhibitory concentration of tobramycin in the supernatant clearly retards growth and development of static biofilms independent of strain and surface mucin patterning. This is evidenced by the delayed onset of PQS production (72 h in the presence of tobramycin) relative to comparable biofilms in the absence of tobramycin (7 to 24 h). Next, we observe clear differences in the behavior of FRD1 and PAO1C strains with the non-mucoid PAO1C strain being much more sensitive to the presence of surface patterning. Third, pyocyanin is observed both in the supernatant and the pellicle biofilm, but not in the static biofilm, strongly suggesting that they are secreted in the pellicle biofilm as a

specific stress response. Finally, under similar conditions, rhamnolipids are expressed at much higher levels in PAO1C than in FRD1.

Irreversible bacterial attachment on the surface is an early step in biofilm formation.[21, 56] Specifically, in the case of CF lung surface, mucin-derived monosaccharides, which are exploited by *P. aeruginosa* to kill other bacteria, are known to influence cell adhesion and increase motility.[57] The present study highlights that mucin patterning is important for PAO1C, for which exopolysaccharide production will be dominated by Pel and Psl. However, the FRD1 strain isolated from the sputum of a CF patient[58], which is known to overproduce alginate, is relatively insensitive to the presence and patterning of mucin. The different behaviors expressed by these strains in response to the spatial patterning in the presence of the antibiotic tobramycin correlates with their intrinsic characteristics. *P. aeruginosa* variants that mucoid biofilms originate in the respiratory tract, where interaction with host mucin is abundant, an observation that is consistent with the preference of the mucoid strain for unpatterned mucin surfaces. The PAO1C strain, on the other hand, is a wound isolate that is capable of continued environmental sensing and bridging of compositional gaps.[59] This is consistent with the results that patterned mucin surfaces and gaps do not hinder static biofilm growth in the non-mucoid strain, even in the presence of antibiotic.

Results from this study highlight the effect of spatial patterning on quorum sensing in *P. aeruginosa* biofilms in an environment containing antibiotics. In addition, there are clear context-dependent differences in clustering behavior, which are likely associated with environmental differences that affect biofilm development. Thus, moving forward it will be important to understand the structural heterogeneity of biofilm and cluster-cluster interactions. In addition, the mechanism of communication between the pellicle and static biofilms deserves further study. In

this regard, it will be useful to investigate the impact of relative distance between the patterned biofilm clusters and the response of *P. aeruginosa* to alternative surfaces.

METHODS

Materials. Silicon wafers (3 inch diam.) were obtained from University Wafer, Inc. Gold (99.999% purity pellets) was supplied by Kurt J. Lesker. Photomasks were supplied by Front Range Photomask. SU-8 2050 and SU-8 developer were purchased from MicroChem. Curing agent and poly(dimethylsiloxane) (PDMS) prepolymer were supplied by Dow Corning. Tobramycin (aminoglycoside antibiotic), 11-mercaptoundecanoic acid (MUA), ethyl alcohol (200 proof), 2-(N-morpholino)ethanesulfonic acid (MES) hydrate, tris (2-carboxyethyl) phosphine hydrochloride (TCEP), pyocyanin (PYO), 2-heptyl-4-hydroxyquinoline N-oxide (HQNO), 2-heptyl-3-hydroxy-4-quinolone (C_7-PQS), 5-dihydroxybenzoic acid (DHB), and mucin from porcine stomach (type III, bound sialic acid 0.5 – 1.5%) were supplied by Sigma-Aldrich. 2-nonyl-4-hydroxyquinoline N-oxide (NQNO) and 2-nonyl-3-hydroxy-4-quinolone (C_9-PQS) were obtained from Cayman Chemical. Phenazine-1-carboxylic acid (PZCA) was purchased from SynQuest Laboratories. Poly(ethylene glycol) (PEG) thiol (MW 550 Da) was supplied by Creative PEGWorks. EDC (1-ethyl-3-[3-(dimethylamino)propyl] carbodiimide hydrochloride) and NHS (N-hydroxysuccinimide) were supplied by Thermo Fisher Scientific. Double-sided copper conducting tape was purchased from 3M. Milli-Q deionized (DI) water ($\rho \sim$ 18.2 MΩ cm) was prepared by a Milli-Q gradient water purification system and used in all cases. All chemicals were used as received.

Substrate Fabrication. The patterned mucin substrate was fabricated by sequential thermal evaporation of gold (50 nm) on silicon, transferring patterned MUA onto the gold

surface using PDMS stamp, coating the remaining gold surface with PEG, and immobilizing mucin via EDC/NHS cross-linking following the procedures described previously.[24] The unpatterned mucin substrate was prepared by coating gold surfaces with MUA (1 mM) followed by immobilizing mucin via EDC/NHS cross-linking. Wafers were rinsed with DI water and dried with N_2 gas after each step.

Biofilm Preparation. *P. aeruginosa* mucoid strain FRD1 and non-mucoid strain PAO1C (ATCC15692) were used in these experiments. The general biofilm preparation strategy is outlined in **Figure 1**. Bacteria from frozen stocks were inoculated on lysogeny broth (LB) agar plates and incubated at 37ºC for 18 h. A single colony was transferred, well-dispersed, and grown planktonically in minimal medium containing 30 mM filtered sterile glucose as the sole carbon source with shaking (240 rpm) at 37ºC for 18 h.[24] Planktonic cultures were then diluted to OD_{600} = 0.3 in fresh minimal medium. To prepare static biofilms, 200 μL of diluted culture was drop cast onto either patterned or unpatterned mucin-modified silicon wafers, then placed in a Petri dish, and 10 min was allowed for bacterial attachment. After gently rinsing, these inoculated wafers were fully immersed in fresh minimal-glucose medium (18 mL) in a sterile Petri dish and incubated at 37ºC for 1 h to form cell clusters. The wafers were then transferred into a new Petri dish containing fresh minimal-glucose medium (18 mL) and tobramycin (5 μg mL^{-1}) and incubated at 37ºC for the desired growth time. A suitable sub-lethal drug concentration level for experiments was determined by evaluating outcomes of various concentrations of tobramycin on *P. aeruginosa* cultures.(See **Supporting Information**, **SI**, for details of the determination of the sub-lethal tobramycin concentration). To collect the static biofilm samples, sterile tweezers were used to carefully remove the wafers from the Petri dish, and samples were air-dried in a fume hood overnight. Pellicle biofilms also formed at the air-water interface of the

supernatant over the static biofilms. These pellicles were collected and transferred onto a sterile gold-coated silicon wafer and allowed to air-dry overnight in a fume hood. planktonic cell cultures were collected from the volume below the pellicle adjacent to areas containing the submerged wafers and centrifuged at 15,000 rpm for 3 min, and the resulting supernatant was collected and filtered through 0.2 μm sterile syringe filters to remove any remaining cells. Finally, the filtered supernatant was drop cast onto a sterile gold-coated silicon wafer and allowed to air-dry overnight in a fume hood. At least three biological replicates were prepared per sample condition per strain. An Eppendorf BioPhotometer plus was used to measure OD_{600} values for all cell culture samples, with minimal medium as a reference sample.

Raman Imaging. Raman images were collected using a confocal Raman microscope (Alpha 300R, WITec) equipped with a 785 nm laser and a 40 × (NA = 0.6) objective. Six to ten Raman images were acquired from each bacterial sample with a full Raman spectrum from each image pixel (60 × 60 pixels over a 25 × 25 μm region) with an integration time of 100 ms/spectrum. Raman images were typically calculated over a spectral range of 1330 cm^{-1} to 1380 cm^{-1}, centered on the characteristic quinolone ring breathing mode, and filtered to generate Raman images. Additional data analysis was performed on the Raman images using the software WITec project 2.1. Principal component analysis (PCA) was used to analyze the Raman hyperspectral data sets using custom analysis codes written in MATLAB (Mathworks Inc.). PCA score images were pre-processed to remove chemically irrelevant features, such as cosmic ray spikes, prior to analysis. All the identifications and assignments of specific compounds were performed as described previously[24, 60] and confirmed with Raman spectra of chemical standards and with correlated MS data.

MALDI-MS Analysis. Samples were anchored on the MALDI target plate with double-sided copper tape. The sample surface was uniformly coated with 40 mg/ml 2,5-dihydroxy benzoic acid prepared in 50% methanol/water with an HTX M5 sprayer. The nozzle was set at 40 mm height with lateral movement speed of 10 mm/sec and flow rate at 0.05 µL/min. Nozzle temperature and stage temperature were set at 70 °C and 30 °C, respectively, before beginning matrix application. Matrix was applied in 4 passes for each sample with intermittent drying for 10 s between passes. Subsequently, the target plates were scanned using a flatbed document scanner at 1200 dpi to facilitate MSI. The scanned images were used to precisely select the target sample area for MSI data acquisition on a MALDI solariX XR 7T FTICR mass spectrometer (Bruker Corp, Billerica, MA). Regions for MSI were selected in FlexImaging (version 5.0, build 89, Bruker), and data were acquired with the help of ftmsControl (version 2.3.0, build 59, Bruker) in positive ion mode using the "ultra-wide" laser setting (~100 µm lateral resolution) and 1M size (transient data points). The excitation laser was operated at 12% and 17% energy at 1000 Hz for MS and MS/MS, respectively. Tandem MS (collision energy 30 eV, isolation width ±1.0 Da) was performed to differentiate PQS (*m/z* 260.165>175.062) and C_9-PQS (*m/z* 288.195>175.062) from their structural isomers HQNO (*m/z* 260.165>159.067) and NQNO (*m/z* 288.195>159.067) as described preciously.[24, 61] Separately, high resolution full-scan imaging data was acquired (*m/z* 100-1100) to monitor various rhamnolipid congeners. Targeted MS/MS data were normalized by maximum average intensity separately for each replicate and sample type. Full-scan data were normalized to total ion chromatogram (TIC) and maximum average (per replicate, per sample type) intensity before further analysis. Extracted ion profiles generated using ±5 ppm extraction window around each *m/z* were used to visualize spatial distribution of these molecules on the sample surfaces. All MSI data analyzed using SCiLS Lab software

(version 2021b, build 9.01.12514), MSI reader (v1.02), R (4.1.2) and Microsoft excel.[62-63] Error bars in plots indicate standard deviation of average intensities from three biological replicates. Student's t-test was performed to estimate the p-values. Principal component analysis plots were generated using ClustVis web tool.[64]

Supporting Information

The Supporting Information is available free of charge. Additional experimental details and characterization, including selection of tobramycin concentration, optical images of static biofilms, OD_{600} value of supernatant of culture medium, principal component analysis of four biomolecules, table listing characteristic features of biomolecules detected by CRM and table listing characteristic features of rhamnolipids detected by MALDI-MS.

Data availability.

MSI data that support the findings of this study are openly available through Illinois databank at https://doi.org/10.13012/B2IDB-0382919_V1.

Acknowledgements

The fabrication of substrates and bacteria sample preparation were supported by the National Science Foundation through grant 1904196, and the CRM analysis and mass spectrometry imaging were supported by National Institute of Allergies and Infectious Diseases by grant R01AI113219-06. The authors gratefully acknowledge Notre Dame Nanofabrication Facility and Integrated Imaging Facility for providing fabrication and characterization support.

Author information

Corresponding Author

*E-mail: pbohn@nd.edu. Tel.: +1 574 631 1849. Fax: +1 574 631 8366.

ORCID

Jin Jia: 0000-0002-2194-5607

Dharmeshkumar Parmar: 0000-0001-7956-7429

Joanna F. Ellis: 0000-0003-4807-6840

Tianyuan Cao: 0000-0002-5854-1972

Allison R. Cutri: 0000-0001-6415-3741

Joshua D. Shrout: 0000-0001-9509-2187

Jonathan V. Sweedler: 0000-0003-3107-9922

Paul W. Bohn: 0000-0001-9052-0349

Author contributions

†Jin Jia and Dharmeshkumar Parmar contributed equally to this work.

JJ designed the experiments, helped to write the manuscript, fabricated the substrates, prepared the biofilms, and performed CRM. DP and JFE performed MSI and helped to write the manuscript. TYC and ARC assisted with substrate fabrication and CRM. JDS, JVS, and PWB helped to design the experiments and write the manuscript. JJ, DP, JDS, JVS and PWB wrote the manuscript. All authors edited the manuscript.

Competing financial interest: The authors declare no competing financial interest.

REFERENCES:

1. Munita, J. M.; Arias, C. A., Mechanisms of Antibiotic Resistance. *Microbiol Spectr* **2016,** *4* (2), 10.1128/microbiolspec.VMBF-0016-2015. DOI: 10.1128/microbiolspec.VMBF-0016-2015.

2. Antonoplis, A.; Zang, X.; Huttner, M. A.; Chong, K. K. L.; Lee, Y. B.; Co, J. Y.; Amieva, M. R.; Kline, K. A.; Wender, P. A.; Cegelski, L., A Dual-Function Antibiotic-Transporter Conjugate Exhibits Superior Activity in Sterilizing MRSA Biofilms and Killing Persister Cells. *J. Am. Chem. Soc.* **2018,** *140* (47), 16140-16151. DOI: 10.1021/jacs.8b08711.

3. Stewart, P. S.; William Costerton, J., Antibiotic Resistance of Bacteria in Biofilms. *The Lancet* **2001,** *358* (9276), 135-138. DOI: https://doi.org/10.1016/S0140-6736(01)05321-1.

4. Huigens, R. W.; Richards, J. J.; Parise, G.; Ballard, T. E.; Zeng, W.; Deora, R.; Melander, C., Inhibition of Pseudomonas aeruginosa Biofilm Formation with Bromoageliferin Analogues. *J. Am. Chem. Soc.* **2007,** *129* (22), 6966-6967. DOI: 10.1021/ja069017t.

5. Wagner, V. E.; Bushnell, D.; Passador, L.; Brooks, A. I.; Iglewski, B. H., Microarray Analysis of Pseudomonas aeruginosa Quorum-sensing Regulons: Effects of Growth Phase and Environment. *J. Bacteriol.* **2003,** *185* (7), 2080. DOI: 10.1128/JB.185.7.2080-2095.2003.

6. Ng, W.-L.; Bassler, B. L., Bacterial Quorum-sensing Network Architectures. *Annu. Rev. Genet.* **2009,** *43*, 197-222. DOI: 10.1146/annurev-genet-102108-134304.

7. O'Loughlin, C. T.; Miller, L. C.; Siryaporn, A.; Drescher, K.; Semmelhack, M. F.; Bassler, B. L., A Quorum-sensing Inhibitor Blocks Pseudomonas aeruginosa Virulence and Biofilm Formation. *Proc. Natl. Acad. Sci. U. S. A.* **2013,** *110* (44), 17981. DOI: 10.1073/pnas.1316981110.

8. Chen, X.; Schauder, S.; Potier, N.; Van Dorsselaer, A.; Pelczer, I.; Bassler, B. L.; Hughson, F. M., Structural Identification of a Bacterial Quorum-sensing Signal Containing Boron. *Nature* **2002,** *415* (6871), 545-549. DOI: 10.1038/415545a.

9. Papenfort, K.; Bassler, B. L., Quorum Sensing Signal–response Systems in Gram-negative Bacteria. *Nat. Rev. Microbiol.* **2016,** *14* (9), 576-588. DOI: 10.1038/nrmicro.2016.89.

10. Yu, Q.; Cho, J.; Shivapooja, P.; Ista, L. K.; Lopez, G. P., Nanopatterned Smart Polymer Surfaces for Controlled Attachment, Killing, and Release of Bacteria. *ACS Appl Mater Interfaces* **2013,** *5* (19), 9295-304. DOI: 10.1021/am4022279.

11. Jiang, Q.; Chen, J.; Yang, C.; Yin, Y.; Yao, K., Quorum Sensing: A Prospective Therapeutic Target for Bacterial Diseases. *Biomed Res. Int.* **2019,** *2019*, 2015978. DOI: 10.1155/2019/2015978.

12. Chuang, S. K.; Vrla, G. D.; Fröhlich, K. S.; Gitai, Z., Surface Association Sensitizes Pseudomonas aeruginosa to Quorum Sensing. *Nat. Commun.* **2019,** *10* (1), 4118. DOI: 10.1038/s41467-019-12153-1.

13. Siryaporn, A.; Kuchma, S. L.; O'Toole, G. A.; Gitai, Z., Surface Attachment Induces Pseudomonas aeruginosa Virulence. *Proc. Natl. Acad. Sci. U. S. A.* **2014,** *111* (47), 16860-16865. DOI: 10.1073/pnas.1415712111.

14. Azam, M. W.; Khan, A. U., Updates on the Pathogenicity Status of Pseudomonas aeruginosa. *Drug Discov. Today* **2019,** *24* (1), 350-359. DOI: https://doi.org/10.1016/j.drudis.2018.07.003.

15. Despotovic, A.; Milosevic, B.; Milosevic, I.; Mitrovic, N.; Cirkovic, A.; Jovanovic, S.; Stevanovic, G., Hospital-acquired Infections in the Adult Intensive Care Unit—Epidemiology, Antimicrobial Resistance Patterns, and Risk Factors for Acquisition and Mortality. *Am. J. Infect. Control* **2020,** *48* (10), 1211-1215. DOI: https://doi.org/10.1016/j.ajic.2020.01.009.

16. Allesen-Holm, M.; Barken, K. B.; Yang, L.; Klausen, M.; Webb, J. S.; Kjelleberg, S.; Molin, S.; Givskov, M.; Tolker-Nielsen, T., A Characterization of DNA Release in Pseudomonas aeruginosa Cultures and Biofilms. *Mol. Microbiol.* **2006,** *59* (4), 1114-1128. DOI: https://doi.org/10.1111/j.1365-2958.2005.05008.x.

17. Lee, J.; Zhang, L., The Hierarchy Quorum Sensing Network in Pseudomonas aeruginosa. *Protein Cell* **2015,** *6* (1), 26-41. DOI: 10.1007/s13238-014-0100-x.

18. Kostylev, M.; Kim, D. Y.; Smalley, N. E.; Salukhe, I.; Greenberg, E. P.; Dandekar, A. A., Evolution of the Pseudomonas aeruginosa Quorum-sensing Hierarchy. *Proc. Natl. Acad. Sci. U. S. A.* **2019,** *116* (14), 7027. DOI: 10.1073/pnas.1819796116.

19. Lin, J.; Cheng, J.; Wang, Y.; Shen, X., The Pseudomonas Quinolone Signal (PQS): Not Just for Quorum Sensing Anymore. *Front. Cell. Infect. Microbiol.* **2018,** *8*, 230-230. DOI: 10.3389/fcimb.2018.00230.

20. Brouwer, S.; Pustelny, C.; Ritter, C.; Klinkert, B.; Narberhaus, F.; Häussler, S., The PqsR and RhlR Transcriptional Regulators Determine the Level of Pseudomonas Quinolone Signal Synthesis in Pseudomonas aeruginosa by Producing Two Different pqsABCDE mRNA Isoforms. *J. Bacteriol.* **2014,** *196* (23), 4163-4171. DOI: 10.1128/JB.02000-14.

21. Wood, T. L.; Gong, T.; Zhu, L.; Miller, J.; Miller, D. S.; Yin, B.; Wood, T. K., Rhamnolipids from Pseudomonas aeruginosa Disperse the Biofilms of Sulfate-reducing Bacteria. *NPJ Biofilms Microbiomes* **2018,** *4*, 22-22. DOI: 10.1038/s41522-018-0066-1.

22. Landry, R. M.; An, D.; Hupp, J. T.; Singh, P. K.; Parsek, M. R., Mucin–Pseudomonas aeruginosa Interactions Promote Biofilm Formation and Antibiotic Resistance. *Mol. Microbiol.* **2006,** *59* (1), 142-151. DOI: https://doi.org/10.1111/j.1365-2958.2005.04941.x.

23. Welsh, M. A.; Eibergen, N. R.; Moore, J. D.; Blackwell, H. E., Small Molecule Disruption of Quorum Sensing Cross-Regulation in Pseudomonas aeruginosa Causes Major and Unexpected Alterations to Virulence Phenotypes. *J. Am. Chem. Soc.* **2015,** *137* (4), 1510-1519. DOI: 10.1021/ja5110798.

24. Jia, J.; Ellis, J. F.; Cao, T.; Fu, K.; Morales-Soto, N.; Shrout, J. D.; Sweedler, J. V.; Bohn, P. W., Biopolymer Patterning-Directed Secretion in Mucoid and Nonmucoid Strains of *Pseudomonas aeruginosa* Revealed by Multimodal Chemical Imaging. *ACS Infect. Dis.* **2021,** *7* (3), 598-607. DOI: 10.1021/acsinfecdis.0c00765.

25. Fothergill, J. L.; Neill, D. R.; Loman, N.; Winstanley, C.; Kadioglu, A., Pseudomonas aeruginosa Adaptation in the Nasopharyngeal Reservoir Leads to Migration and Persistence in the Lungs. *Nat. Commun.* **2014,** *5* (1), 4780. DOI: 10.1038/ncomms5780.

26. Gu, H.; Hou, S.; Yongyat, C.; De Tore, S.; Ren, D., Patterned Biofilm Formation Reveals a Mechanism for Structural Heterogeneity in Bacterial Biofilms. *Langmuir* **2013,** *29* (35), 11145-11153. DOI: 10.1021/la402608z.

27. Bjarnsholt, T.; Jensen, P.; Fiandaca, M.; Pedersen, J.; Hansen , C.; Andersen, C.; Pressler, T.; Givskov, M.; Hoiby, N., Pseudomonas aeruginosa Biofilms in the Respiratory Tract of Cystic Fibrosis Patients. *Pediatr. Pulmonol.* **2009,** *44*, 547-558.

28. Ohman, D. E.; Chakrabarty, A. M., Genetic Mapping of Chromosomal Determinants for the Production of the Exopolysaccharide Alginate in a Pseudomonas aeruginosa Cystic Fibrosis Isolate. *Infect Immun* **1981,** *33* (1), 142-8. DOI: 10.1128/iai.33.1.142-148.1981.

29. Leid, J. G.; Willson, C. J.; Shirtliff, M. E.; Hassett, D. J.; Parsek, M. R.; Jeffers, A. K., The Exopolysaccharide Alginate Protects *Pseudomonas aeruginosa* Biofilm Bacteria from IFN-Gamma-mediated Macrophage Killing. *J. Immunol.* **2005,** *175* (11), 7512-8. DOI: 175/11/7512 [pii].

30. Pham, T. H.; Webb, J. S.; Rehm, B. H., The Role of Polyhydroxyalkanoate Biosynthesis by *Pseudomonas aeruginosa* in Rhamnolipid and Alginate Production as well as Stress Tolerance and Biofilm Formation. *Microbiology* **2004,** *150* (Pt 10), 3405-13.

31. Tart, A. H.; Blanks, M. J.; Wozniak, D. J., The AlgT-dependent Transcriptional Regulator AmrZ (AlgZ) Inhibits Flagellum Biosynthesis in Mucoid, Nonmotile *Pseudomonas aeruginosa* Cystic Fibrosis Isolates. *J. Bacteriol.* **2006,** *188* (18), 6483-9. DOI: 188/18/6483 [pii] 10.1128/JB.00636-06.

32. Wyckoff, T. J.; Thomas, B.; Hassett, D. J.; Wozniak, D. J., Static Growth of Mucoid *Pseudomonas aeruginosa* Selects for Non-mucoid Variants that Have Acquired Flagellum-dependent Motility. *Microbiology* **2002,** *148* (Pt 11), 3423-30.

33. Morris, J. D.; Hewitt, J. L.; Wolfe, L. G.; Kamatkar, N. G.; Chapman, S. M.; Diener, J. M.; Courtney, A. J.; Leevy, W. M.; Shrout, J. D., Imaging and Analysis of *Pseudomonas aeruginosa* Swarming and Rhamnolipid Production. *Appl. Environ. Microbiol.* **2011,** *77* (23), 8310-8317. DOI: 10.1128/aem.06644-11.

34. Holloway, B. W., Genetic Recombination in *Pseudomonas aeruginosa*. *J. Gen. Microbiol.* **1955,** *13* (3), 572-581. DOI: 10.1099/00221287-13-3-572.

35. Holloway, B. W.; Krishnapillai, V.; Morgan, A. F., Chromosomal Genetics of *Pseudomonas*. *Microbiology Reviews* **1979,** *43* (1), 73-102.

36. Anyan, M. E.; Amiri, A.; Harvey, C. W.; Tierra, G.; Morales-Soto, N.; Driscoll, C. M.; Alber, M. S.; Shrout, J. D., Type IV Pili Interactions Promote Intercellular Association and Moderate Swarming of *Pseudomonas aeruginosa*. *Proc. Natl. Acad. Sci. U. S. A.* **2014,** *111* (50), 18013-8. DOI: 10.1073/pnas.1414661111.

37. Gibiansky, M. L.; Conrad, J. C.; Jin, F.; Gordon, V. D.; Motto, D. A.; Mathewson, M. A.; Stopka, W. G.; Zelasko, D. C.; Shrout, J. D.; Wong, G. C. L., Bacteria Use Type IV Pili to Walk Upright and Detach from Surfaces. *Science* **2010,** *330* (6001), 197. DOI: 10.1126/science.1194238.

38. Morales-Soto, N.; Dunham, S. J. B.; Baig, N. F.; Ellis, J. F.; Madukoma, C. S.; Bohn, P. W.; Sweedler, J. V.; Shrout, J. D., Spatially Dependent Alkyl Quinolone Signaling Responses to Antibiotics in *Pseudomonas aeruginosa* Swarms. *J. Biol. Chem.* **2018,** *293* (24), 9544-9552. DOI: 10.1074/jbc.RA118.002605.

39. Shrout, J. D.; Chopp, D. L.; Just, C. L.; Hentzer, M.; Givskov, M.; Parsek, M. R., The Impact of Quorum Sensing and Swarming Motility on Pseudomonas aeruginosa Biofilm Formation is Nutritionally Conditional. *Mol. Microbiol.* **2006,** *62* (5), 1264-1277. DOI: Doi 10.1111/J.1365-2958.2006.05421.X.

40. Haley, C. L.; Colmer-Hamood, J. A.; Hamood, A. N., Characterization of Biofilm-like Structures Formed by Pseudomonas aeruginosa in a Synthetic Mucus Medium. *BMC Microbiol.* **2012,** *12* (1), 181. DOI: 10.1186/1471-2180-12-181.

41. Babić, F.; Venturi, V.; Maravić-Vlahoviček, G., Tobramycin at Subinhibitory Concentration Inhibits the RhlI/R Quorum Sensing System in a Pseudomonas aeruginosa Environmental Isolate. *BMC Infect. Dis.* **2010,** *10* (1), 148. DOI: 10.1186/1471-2334-10-148.

42. Brewer, L. K.; Jones, J. W.; Blackwood, C. B.; Barbier, M.; Oglesby-Sherrouse, A.; Kane, M. A., Development and Bioanalytical Method Validation of an LC-MS/MS Assay for Simultaneous Quantitation of 2-alkyl-4(1H)-quinolones for Application in Bacterial Cell Culture and Lung Tissue. *Anal. Bioanal. Chem.* **2020,** *412* (7), 1521-1534. DOI: 10.1007/s00216-019-02374-0.

43. Lépine, F.; Milot, S.; Déziel, E.; He, J.; Rahme, L. G., Electrospray/mass Spectrometric Identification and Analysis of 4-hydroxy-2-Alkylquinolines (HAQs) Produced by *Pseudomonas aeruginosa*. *J. Am. Soc. Mass Spectrom.* **2004,** *15* (6), 862-869. DOI: http://dx.doi.org/10.1016/j.jasms.2004.02.012.

44. Murray, E. J.; Dubern, J.-F.; Chan, W. C.; Chhabra, S. R.; Williams, P., A Pseudomonas aeruginosa PQS Quorum-sensing System Inhibitor with Anti-staphylococcal Activity Sensitizes Polymicrobial Biofilms to Tobramycin. *Cell Chem. Biol.* **2022**. DOI: https://doi.org/10.1016/j.chembiol.2022.02.007.

45. Baig, N. F.; Dunham, S. J. B.; Morales-Soto, N.; Shrout, J. D.; Sweedler, J. V.; Bohn, P. W., Multimodal Chemical Imaging of Molecular Messengers in Emerging *Pseudomonas*

aeruginosa Bacterial Communities. *Analyst* **2015,** *140* (19), 6544-6552. DOI: 10.1039/C5AN01149C.

46. Moreau-Marquis, S.; Stanton, B. A.; O'Toole, G. A., Pseudomonas aeruginosa Biofilm Formation in the Cystic Fibrosis Airway. *Pulm Pharmacol Ther* **2008,** *21* (4), 595-599. DOI: 10.1016/j.pupt.2007.12.001.

47. Venkatesan, N.; Perumal, G.; Doble, M., Bacterial Resistance in Biofilm-associated Bacteria. *Fut. Microbiol.* **2015,** *10* (11), 1743-1750. DOI: 10.2217/fmb.15.69.

48. Elkins, J. G.; Hassett, D. J.; Stewart, P. S.; Schweizer, H. P.; McDermott, T. R., Protective Role of Catalase in Pseudomonas aeruginosa Biofilm Resistance to Hydrogen Peroxide. *Appl. Environ. Microbiol.* **1999,** *65* (10), 4594-4600. DOI: 10.1128/AEM.65.10.4594-4600.1999.

49. Abdel-Mawgoud, A. M.; Lépine, F.; Déziel, E., Rhamnolipids: Diversity of Structures, Microbial Origins and Roles. *Appl. Microbiol. Biotechnol.* **2010,** *86* (5), 1323-1336. DOI: 10.1007/s00253-010-2498-2.

50. Rajput, A.; Thakur, A.; Sharma, S.; Kumar, M., aBiofilm: A Resource of Anti-biofilm Agents and Their Potential Implications in Targeting Antibiotic Drug Resistance. *Nucleic Acids Res.* **2018,** *46* (D1), D894-D900. DOI: 10.1093/nar/gkx1157.

51. Simões, M.; Simões, L. C.; Vieira, M. J., Species Association Increases Biofilm Resistance to Chemical and Mechanical Treatments. *Water Res.* **2009,** *43* (1), 229-237. DOI: https://doi.org/10.1016/j.watres.2008.10.010.

52. Crull, M. R.; Somayaji, R.; Ramos, K. J.; Caldwell, E.; Mayer-Hamblett, N.; Aitken, M. L.; Nichols, D. P.; Rowhani-Rahbar, A.; Goss, C. H., Changing Rates of Chronic Pseudomonas aeruginosa Infections in Cystic Fibrosis: A Population-Based Cohort Study. *Clin. Infect. Dis.* **2018,** *67* (7), 1089-1095. DOI: 10.1093/cid/ciy215.

53. Bhattacharjee, A.; Nusca, T. D.; Hochbaum, A. I., Rhamnolipids Mediate an Interspecies Biofilm Dispersal Signaling Pathway. *ACS Chem. Biol.* **2016,** *11* (11), 3068-3076. DOI: 10.1021/acschembio.6b00750.

54. Calfee, M. W.; Shelton, J. G.; McCubrey, J. A.; Pesci, E. C., Solubility and Bioactivity of the Pseudomonas Quinolone Signal are Increased by a Pseudomonas aeruginosa-produced Surfactant. *Infect. Immun.* **2005,** *73* (2), 878-882. DOI: 10.1128/IAI.73.2.878-882.2005.

55. Davey Mary, E.; Caiazza Nicky, C.; O'Toole George, A., Rhamnolipid Surfactant Production Affects Biofilm Architecture in Pseudomonas aeruginosa PAO1. *J. Bacteriol.* **2003,** *185* (3), 1027-1036. DOI: 10.1128/JB.185.3.1027-1036.2003.

56. Watnick, P.; Kolter, R., Biofilm, City of Microbes. *J. Bacteriol.* **2000,** *182* (10), 2675-2679. DOI: 10.1128/JB.182.10.2675-2679.2000.

57. Yeung Amy, T. Y.; Parayno, A.; Hancock Robert, E. W.; Bush, K., Mucin Promotes Rapid Surface Motility in Pseudomonas aeruginosa. *mBio* **2012,** *3* (3), e00073-12. DOI: 10.1128/mBio.00073-12.

58. Ohman, D. E.; Chakrabarty, A. M., Genetic Mapping of Chromosomal Determinants for the Production of the Exopolysaccharide Alginate in a Pseudomonas aeruginosa Cystic Fibrosis Isolate. *Infect. Immun.* **1981,** *33* (1), 142.

59. Silo-Suh, L. A.; Suh, S.-J.; Ohman, D. E.; Wozniak, D. J.; Pridgeon, J. W., Complete Genome Sequence of Pseudomonas aeruginosa Mucoid Strain FRD1, Isolated from a Cystic Fibrosis Patient. *Genome Announc.* **2015,** *3* (2), e00153-15. DOI: 10.1128/genomeA.00153-15.

60. Jia, J.; Kwon, S.-R.; Baek, S.; Sundaresan, V.; Cao, T.; Cutri, A. R.; Fu, K.; Roberts, B.; Shrout, J. D.; Bohn, P. W., Actively Controllable Solid-Phase Microextraction in a Hierarchically Organized Block Copolymer-Nanopore Electrode Array Sensor for Charge-Selective Detection of Bacterial Metabolites. *Anal. Chem.* **2021,** *93* (43), 14481-14488. DOI: 10.1021/acs.analchem.1c02998.

61. Morales-Soto, N.; Dunham, S. J. B.; Baig, N. F.; Ellis, J. F.; Madukoma, C. S.; Bohn, P. W.; Sweedler, J. V.; Shrout, J. D., Spatially Dependent Alkyl Quinolone Signaling Responses to Antibiotics in Pseudomonas aeruginosa Swarms. *Journal of Biological Chemistry* **2018,** *293* (24), 9544-9552. DOI: 10.1074/jbc.RA118.002605.

62. Robichaud, G.; Garrard, K. P.; Barry, J. A.; Muddiman, D. C., MSiReader: An Open-Source Interface to View and Analyze High Resolving Power MS Imaging Files on Matlab Platform. *J. Am. Soc. Mass Spectrom.* **2013,** *24* (5), 718-721. DOI: 10.1007/s13361-013-0607-z.

63. Bokhart, M. T.; Nazari, M.; Garrard, K. P.; Muddiman, D. C., MSiReader v1.0: Evolving Open-Source Mass Spectrometry Imaging Software for Targeted and Untargeted Analyses. *J. Am. Soc. Mass Spectrom.* **2018,** *29* (1), 8-16. DOI: 10.1007/s13361-017-1809-6.

64. Metsalu, T.; Vilo, J., ClustVis: A Web Tool for Visualizing Clustering of Multivariate Data Using Principal Component Analysis and Heatmap. *Nucleic Acids Res.* **2015,** *43* (W1), W566-W570. DOI: 10.1093/nar/gkv468.

For Table of Contents Use Only

Effect of Micro-patterned Mucin on Quinolone and Rhamnolipid Profiles of Mucoid *Pseudomonas aeruginosa* under Antibiotic Stress

Jin Jia[⊥], Dharmeshkumar Parmar[⊥], Joanna F. Ellis, Tianyuan Cao, Allison R. Cutri, Joshua D. Shrout, Jonathan V. Sweedler, Paul W. Bohn*

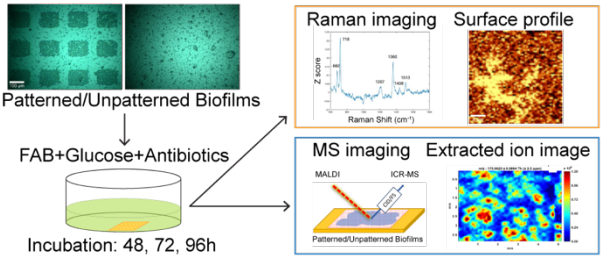

TOC image shows key steps of the sample preparation and analysis workflow. Images from left to right depict media and time points of biofilm sample collection, Raman and mass spectrometry imaging, and extracted Raman and ion images of quinolone signal. Non-destructive confocal Raman imaging was used to characterize various bacterial products. MSI characterization of biofilm surfaces allows assessment of distribution patterns and spatial localization of bacterial signaling molecules. Sequential acquisition of MS data from the sample surface facilitates reconstruction of an image that corresponds to the peak intensities observed per each pixel or location of laser ablation. In our study, we analyzed biomolecules produced by *P. aeruginosa* to understand how the secretion of quinolones and rhamnolipids are impacted by the surface microenvironment in the presence of a sub-inhibitory concentration of antibiotic.

Supporting Information for

Effect of Micro-patterned Mucin on Quinolone and Rhamnolipid Profiles of Mucoid *Pseudomonas aeruginosa* under Antibiotic Stress

Jin Jia[†⊥], *Dharmeshkumar Parmar*[‡⊥], *Joanna F. Ellis*[‡], *Tianyuan Cao*[†], *Allison R. Cutri*[†], *Joshua D. Shrout*[§&], *Jonathan V. Sweedler*[‡], *Paul W. Bohn*[*†£]

[†]Department of Chemistry and Biochemistry, University of Notre Dame, Notre Dame, Indiana 46556, United States

[£]Department of Chemical and Biomolecular Engineering, University of Notre Dame, Notre Dame, Indiana 46556, United States

[‡]Department of Chemistry and Beckman Institute for Advanced Science and Technology, University of Illinois at Urbana−Champaign, Urbana, Illinois 61801, United States

[§]Department of Civil and Environmental Engineering and Earth Sciences, University of Notre Dame, Notre Dame, Indiana 46556, United States

[&]Department of Biological Sciences, University of Notre Dame, Notre Dame, Indiana 46556, United States

[*]Author to whom correspondence should be addressed, *pbohn@nd.edu*.

Table of Contents

Selection of Tobramycin Concentration

P. aeruginosa is an opportunistic pathogen and can cause serious infections in cystic fibrosis (CF) patients and others with burn wounds.[1-2] In the lungs of CF patients, the genetic disorder leads to purulent viscous mucus secretion and impaired mucociliary clearance that promotes bacterial infection, especially by *P. aeruginosa*.[3] Tobramycin, an aminoglycoside antibiotic, is one of the most frequently used antibiotics for CF lung infections caused by *P. aeruginosa*.[4-5] Tobramycin has shown some success in clearing planktonic *P. aeruginosa* cells; however, during chronic infection, *P. aeruginosa* grows as biofilms and shows increasing antibiotic resistance due to gene mutation.[3] Additionally, the viscous mucus environment in CF lungs and the complex three-dimensional structure of the biofilm limit the access of tobramycin to infection sites and greatly reduce its efficacy.

In vitro studies show that 4 μg mL^{-1} tobramycin can reduce the amount of *P. aeruginosa* biofilm by as much as 55%, and tobramycin at ≥ 100 μg mL^{-1} displays strong bactericidal effects.[6] To study the effect of spatial patterning of mucin on QS of *P. aeruginosa* biofilm during antibiotic treatment, it is first necessary to identify a concentration of tobramycin that shows a significant antibacterial effect but does not kill all the cells. To address this question, mucoid (strain FRD1) and nonmucoid (strain PAO1C) *P. aeruginosa* were grown on silicon in minimal-glucose medium containing 0, 0.5, 5, 50, and 500 μg mL^{-1} tobramycin at 37 ºC and sampled at 24, 48, 72, 96, 120, and 144 h.

Samples grown in the presence of 0 and 0.5 μg mL^{-1} tobramycin showed similar turbid blue-green color at 24 h incubation time, indicating the presence of planktonic cells and secreted pigments in the media. The physical similarity of these two samples indicates that 0.5 μg mL^{-1} tobramycin is not sufficient to diminish biofilm growth significantly. Samples grown in the

presence of 50 and 500 μg mL^{-1} tobramycin remained clear, and no color change was observed even after 144 h incubation time, indicating that these two concentrations of tobramycin are sufficient to eradicate the vast majority of *P. aeruginosa* cells. In contrast, samples grown in the presence of 5 μg mL^{-1} tobramycin, exhibited a medium that stayed clear with no color change until 48 h. However, starting at 72 h, the medium became turbid and developed a blue-green color, indicating the presence of planktonic cells and secreted pigments in the medium. The observations that 0.5 μg mL^{-1} did not significantly affect bacterial growth, and concentrations ≥ 50 μg mL^{-1} killed all bacterial cells in the system established a concentration window for these studies. Thus, 5 μg mL^{-1} tobramycin was observed to greatly reduce biofilm growth without completely eradicating all the *P. aeruginosa* cells, *i.e.*, sub-inhibitory behavior, making it the preferred tobramycin concentration for the experiments probing the effect of patterned mucin surfaces on QS of *P. aeruginosa* biofilms under antibiotic stress conditions.

FIGURES AND TABLES

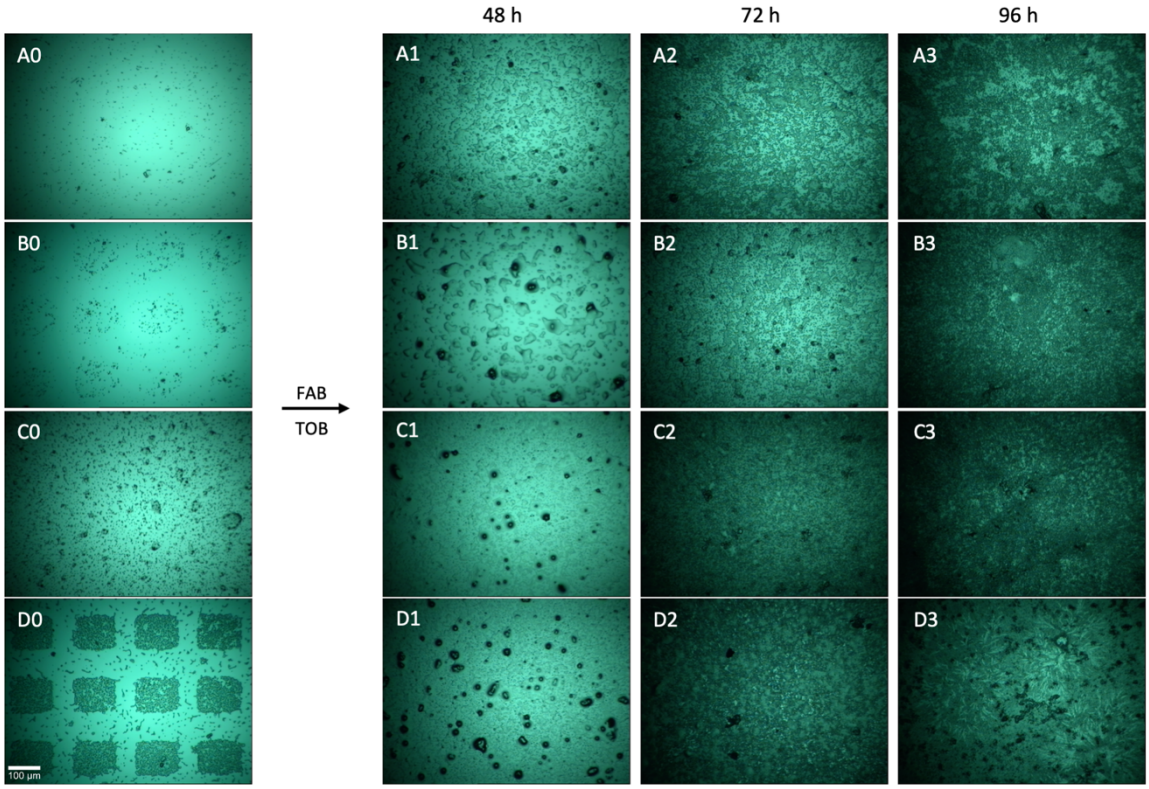

Figure S1. Representative optical images of *P. aeruginosa* static biofilm growth under antibiotic treatment conditions on patterned and unpatterned mucin surfaces. Column 0 is static bacterial biofilm after 1 h incubation in minimal-glucose medium without tobramycin. Columns 1, 2, and 3 are static bacterial biofilms grown in minimal-glucose medium in the presence of tobramycin for 48 h (column 1), 72 h (column 2), and 96 h (column 3). Row A is obtained from static biofilms of the mucoid phenotype on an unpatterned mucin surface. Row B is obtained from static biofilms of the mucoid phenotype on a patterned mucin surface. Row C is obtained from static biofilms of the nonmucoid phenotype on an unpatterned mucin surface. Row D is obtained from static biofilms of the nonmucoid phenotype on a patterned mucin surface. (Scale bar = 100 µm, all images at the same magnification)

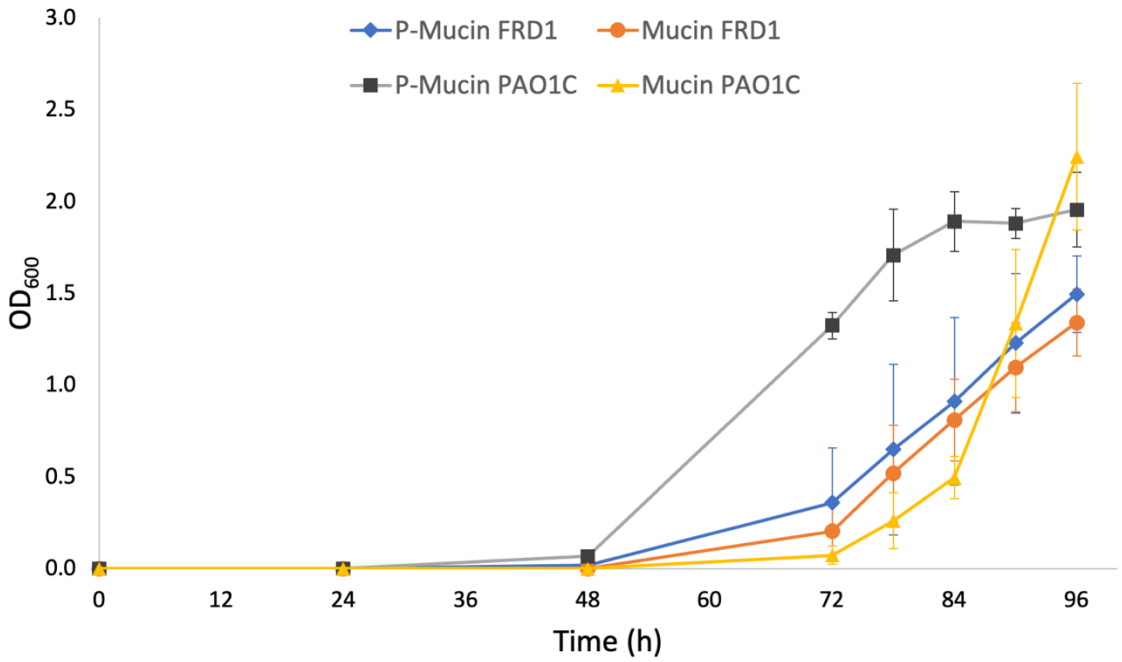

Figure S2. OD_{600} values of the supernatant from various culture media as a function of time of bacterial incubation. "P-Mucin" denotes patterned mucin surfaces, and "Mucin" denotes unpatterned surfaces.

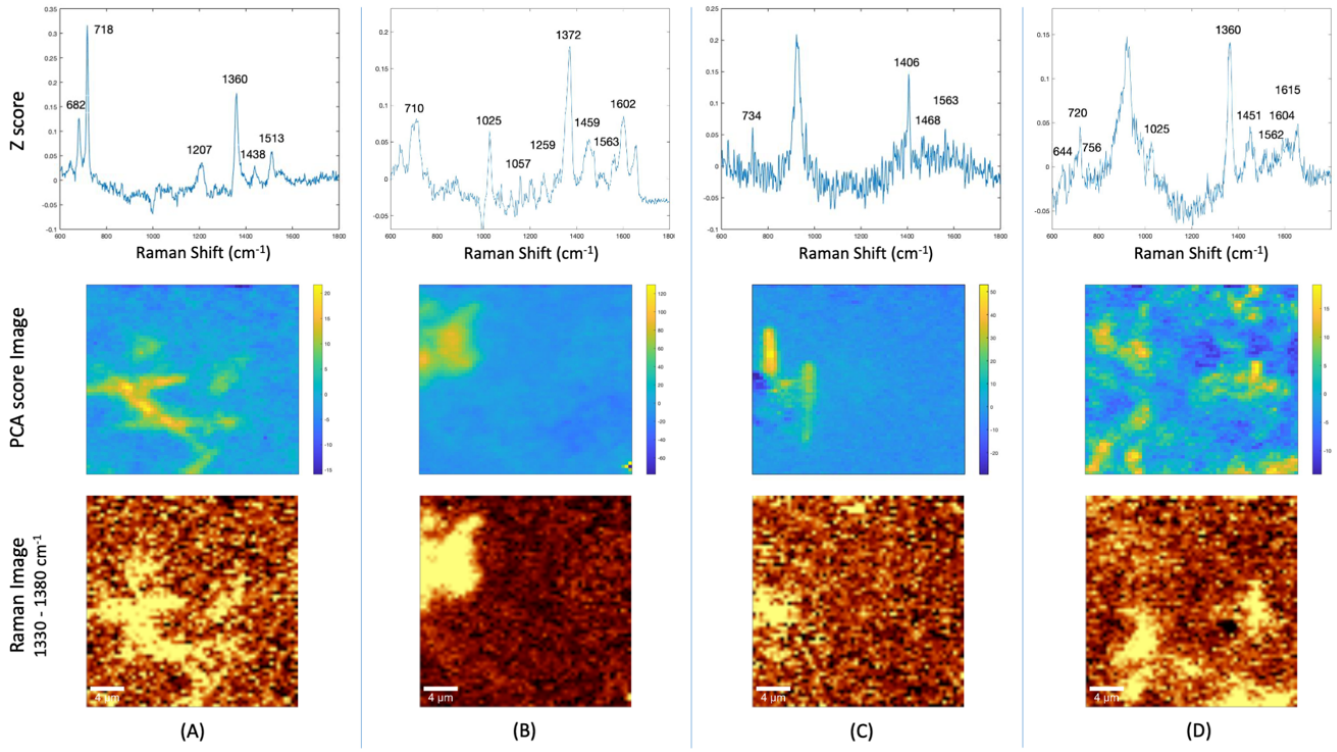

Figure S3. PCA of representative CRM images of *P. aeruginosa* biofilms identifying four molecular constituents. (Top row) PCA loading plots show the z-score *vs*. Raman shift for the highest ranking principal component. (Middle row) PCA score images show the spatial distribution and magnitude of the highest ranking principal component. (Bottom row) Raman images showing intensities integrated over 1330-1380 cm^{-1}. PCA loading plot, score image, and Raman image in each column were acquired from the same sample. (A) 72 h PAO1C static biofilm on P-Mucin; loading plot dominated by N/HQNO. (B) 96 h FRD1 pellicle biofilm on gold surface; loading plot dominated by PQS. (C) 96 h PAO1C bacteria-free supernatant; loading plot dominated by PZCA. (D) 96 h PAO1C pellicle biofilm; loading plot dominated by PYO. (scale bar = 4 µm)

Table S1. Raman bands in chemical standards by CRM

Compounds	Raman Standard Band Positions (cm^{-1})
H/NQNO Standard	681, 720, 1201, 1358, 1441, 1514
PQS Standard	620, 711, 1028, 1156, 1224, 1260, 1375, 1461, 1561, 1601
PZCA Standard	736, 1406, 1468, 1562
PYO Standard	644, 699, 752, 1032, 1357, 1462, 1494, 1565, 1602, 1613

Table S2. List of rhamnolipids congeners detected by MALDI-MS in positive ion mode[a]

Rhamnolipid	Adduct	*m/z*
Rha-C8:2	$[M+Na]^+$	325.1258
Rha-C8:2	$[M+K]^+$	341.0997
Rha-C10	$[M+Na]^+$	357.1884
Rha-C12:2	$[M+Na]^+$	381.1884^+
Rha-C12	$[M+Na]^+$	385.2197
Rha-C12	$[M+K]^+$	401.1936
Rha-C14:2	$[M+Na]^+$	409.2197
Rha-Rha-C8	$[M+H]^+$	453.233
Rha-C16	$[M+Na]^+$	471.2565
Rha-Rha-C10	$[M+H]^+$	481.2643
Rha-Rha-C8	$[M+K]^+$	491.1889
Rha-C18	$[M+Na]^+$	499.2878
Rha-C18	$[M+K]^+$	515.2617

Rha-Rha-C10	$[M+K]^+$	519.2202
Rha-C20:1	$[M+Na]^+$	525.3034
Rha-C20	$[M+Na]^+$	527.3191
Rha-C20	$[M+K]^+$	543.293
Rha-C22:1	$[M+Na]^+$	553.3347
Rha-C22	$[M+Na]^+$	555.3504
Rha-C24:1	$[M+H]^+$	559.3841
Rha-C24	$[M+H]^+$	561.3997
Rha-C22:1	$[M+K]^+$	569.3086
Rha-C22	$[M+K]^+$	571.3243
Rha-Rha-C16	$[M+H]^+$	595.3324
Rha-Rha-C18	$[M+H]^+$	623.3637
Rha-Rha-C18	$[M+Na]^+$	645.3457
Rha-Rha-C18	$[M+K]^+$	661.3196
Rha-Rha-C20	$[M+Na]^+$	673.377
Rha-Rha-C20	$[M+K]^+$	689.3509
Rha-Rha-C22:1	$[M+Na]^+$	699.3926
Rha-Rha-C22	$[M+Na]^+$	701.4083
Rha-Rha-C22:1	$[M+K]^+$	715.3666
Rha-Rha-C22	$[M+K]^+$	717.3822
Rha-Rha-C24:1	$[M+Na]^+$	727.4239
Rha-Rha-C24	$[M+Na]^+$	729.4396
Rha-Rha-C24:1	$[M+K]^+$	743.3979

Rha-Rha-C24	$[M+K]^+$	745.4135
Decenoyl-Rha-Rha-C20	$[M+Na]^+$	825.4971

[a] All adducts were detected within ±5 ppm mass accuracy.

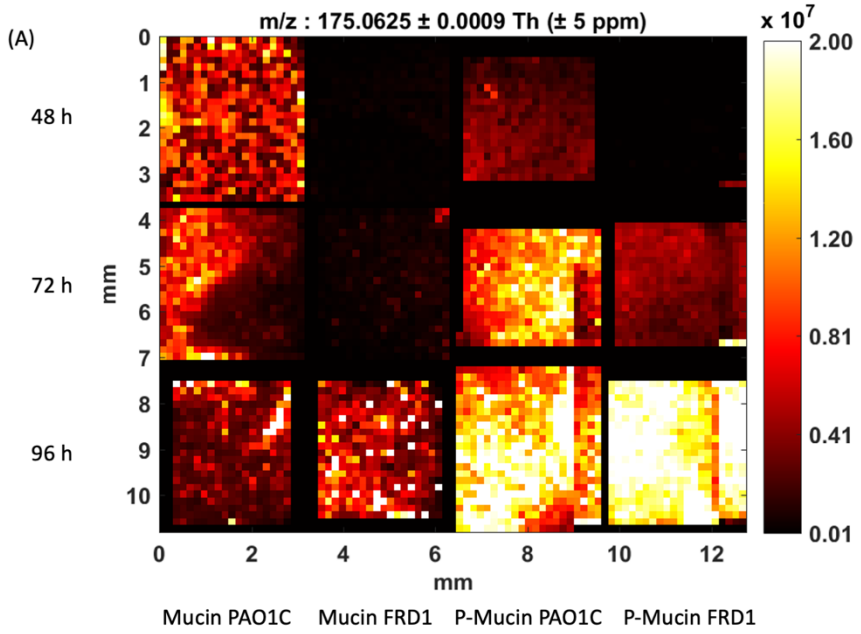
(A)
m/z : 175.0625 ± 0.0009 Th (± 5 ppm)
x 10^7
2.00
1.60
1.20
0.81
0.41
0.01
48 h
72 h
96 h
mm
0 1 2 3 4 5 6 7 8 9 10
0 2 4 6 8 10 12
mm
Mucin PAO1C
Mucin FRD1
P-Mucin PAO1C
P-Mucin FRD1

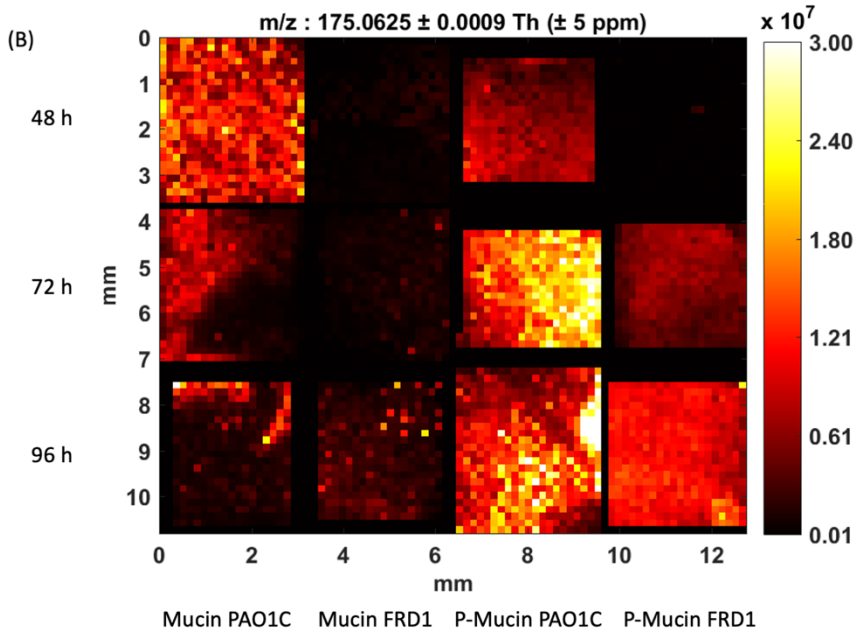
(B)
m/z : 175.0625 ± 0.0009 Th (± 5 ppm)
x 10^7
3.00
2.40
1.80
1.21
0.61
0.01
48 h
72 h
96 h
mm
0 1 2 3 4 5 6 7 8 9 10
0 2 4 6 8 10 12
mm
Mucin PAO1C
Mucin FRD1
P-Mucin PAO1C
P-Mucin FRD1

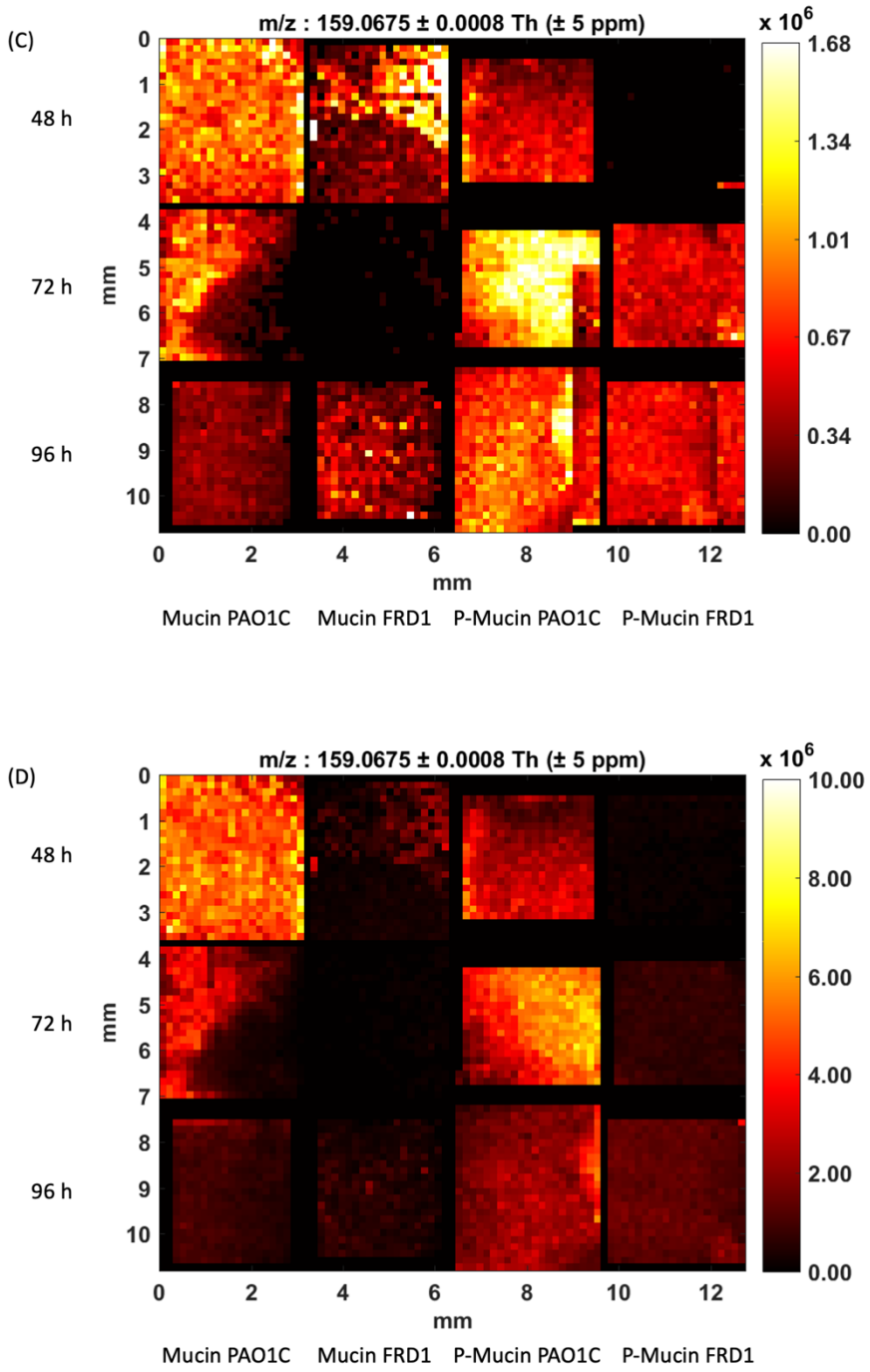

Figure S4. Extracted ion images (with scale for intensity color gradient) of PQS and AQNO molecules from *P. aeruginosa* static biofilms. (A) PQS (*m/z* 260→175), (B) C9-PQS (*m/z* 288→175), (C) HQNO (*m/z* 260→159), and (D) NQNO (*m/z* 288→159). Extracted ion images

were generated using ± 5 ppm extraction window around the observed *m/z* value. Rows represent sample collection times, and columns represent strain and type of mucin surface.

REFERENCES:

1. Gooderham, W. J.; Hancock, R. E. W., Regulation of Virulence and Antibiotic Resistance by Two-component Regulatory Systems in Pseudomonas aeruginosa. *FEMS Microbiol. Rev.* **2009,** *33* (2), 279-294.

2. Bjarnsholt, T.; Jensen, P. Ø.; Fiandaca, M. J.; Pedersen, J.; Hansen, C. R.; Andersen, C. B.; Pressler, T.; Givskov, M.; Høiby, N., Pseudomonas aeruginosa Biofilms in the Respiratory Tract of Cystic Fibrosis Patients. *Pediatr. Pulmonol.* **2009,** *44* (6), 547-558.

3. Fothergill, J. L.; Neill, D. R.; Loman, N.; Winstanley, C.; Kadioglu, A., Pseudomonas aeruginosa Adaptation in the Nasopharyngeal Reservoir Leads to Migration and Persistence in the Lungs. *Nat. Commun.* **2014,** *5* (1), 4780.

4. Anwar, H.; Strap, J. L.; Chen, K.; Costerton, J. W., Dynamic Interactions of Biofilms of Mucoid Pseudomonas aeruginosa with Tobramycin and Piperacillin. *Antimicrob. Agents Chemother.* **1992,** *36* (6), 1208.

5. Nickel, J. C.; Ruseska, I.; Wright, J. B.; Costerton, J. W., Tobramycin Resistance of Pseudomonas aeruginosa Cells Growing as a Biofilm on Urinary Catheter Material. *Antimicrob. Agents Chemother.* **1985,** *27* (4), 619.

6. Thellin, O.; Zorzi, W.; Jolois, O.; Elmoualij, B.; Duysens, G.; Cahay, B.; Streel, B.; Charif, M.; Bastin, R.; Heinen, E.; Quatresooz, P., In Vitro Approach to Study the Synergistic Effects of Tobramycin and Clarithromycin Against Pseudomonas aeruginosa Biofilms Using Prokaryotic or Eukaryotic Culture Media. *Int. J. Antimicrob. Agents* **2015,** *46* (1), 33-38.